Vol.7, May.2014 ISSN 2354-7065

Journal of

Ocean, Mechanical and Aerospace

-Science and Engineering-

ISOMAse

International Society of Ocean, Mechanical and Aerospace,
Scientists and Engineers

Journal of Ocean, Mechanical and Aerospace
-Science and Engineering-
Vol.7: May 2014

Contents

Call for Papers on Ocean, Mechanical and Aerospace "Scientists and Engineers" (OMAse) 2014

ISOMAse

International Society of Ocean, Mechanical and Aerospace
-Scientists and Engineers-

Journal of Ocean, Mechanical and Aerospace
-Science and Engineering-
Vol.7: May 2014

About JOMAse

The **Journal of Ocean, Mechanical and Aerospace -science and engineering- (JOMAse, ISSN: 2354-7065)** is an online professional journal which is published by the International Society of Ocean, Mechanical and Aerospace -scientists and engineers- (ISOMAse), Insya Allah, twelve volumes in a year. The mission of the JOMAse is to foster free and extremely rapid scientific communication across the world wide community. The JOMAse is an original and peer review article that advance the understanding of both science and engineering and its application to the solution of challenges and complex problems in naval architecture, offshore and subsea, machines and control system, aeronautics, satellite and aerospace. The JOMAse is particularly concerned with the demonstration of applied science and innovative engineering solutions to solve specific industrial problems. Original contributions providing insight into the use of computational fluid dynamic, heat transfer, thermodynamics, experimental and analytical, application of finite element, structural and impact mechanics, stress and strain localization and globalization, metal forming, behaviour and application of advanced materials in ocean and aerospace engineering, robotics and control, tribology, materials processing and corrosion generally from the core of the journal contents are encouraged. Articles preferably should focus on the following aspects: new methods or theory or philosophy innovative practices, critical survey or analysis of a subject or topic, new or latest research findings and critical review or evaluation of new discoveries. The authors are required to confirm that their paper has not been submitted to any other journal in English or any other language.

ISOMAse

International Society of Ocean, Mechanical and Aerospace
-Scientists and Engineers-

Journal of Ocean, Mechanical and Aerospace
-Science and Engineering-
Vol.7: May 2014

Scope of JOMAse

The JOMAse welcomes manuscript submissions from academicians, scholars, and practitioners for possible publication from all over the world that meets the general criteria of significance and educational excellence. The scope of the journal is as follows:

- Environment and Safety
- Renewable Energy
- Naval Architecture and Offshore Engineering
- Computational and Experimental Mechanics
- Hydrodynamic and Aerodynamics
- Noise and Vibration
- Aeronautics and Satellite
- Engineering Materials and Corrosion
- Fluids Mechanics Engineering
- Stress and Structural Modeling
- Manufacturing and Industrial Engineering
- Robotics and Control
- Heat Transfer and Thermal
- Power Plant Engineering
- Risk and Reliability
- Case studies and Critical reviews

The International Society of Ocean, Mechanical and Aerospace –science and engineering is inviting you to submit your manuscript(s) to isomase.org@gmail.com for publication. Our objective is to inform authors of the decision on their manuscript(s) within 2 weeks of submission. Following acceptance, a paper will normally be published in the next online issue.

ISOMAse

International Society of Ocean, Mechanical and Aerospace
-Scientists and Engineers-

Journal of Ocean, Mechanical and Aerospace
-Science and Engineering-
Vol.7: May 2014

Editors

Published in Indonesia.

JOMAse

ISOMAse,
Jalan Sisingamangaraja No.89
Pekanbaru-Riau
Indonesia
http://www.isomase.org/

Printed in Indonesia.

Teknik Mesin
Fakultas Teknik
Universitas Riau, Indonesia
http://ft.unri.ac.id/

ISOMAse

International Society of Ocean, Mechanical and Aerospace
-Scientists and Engineers-

Journal of Ocean, Mechanical and Aerospace
-Science and Engineering-, Vol.7

May 20, 2014

Structural Sensitivity of Tarpon Monopods in Intermediate Water Depths for Marginal Field Development

Lee Hsiu Eik[a,*] and Mohd Shahir Liew,[a]

[a)]*Department of Civil Engineering, Universiti Teknologi PETRONAS ,Bandar Seri Iskandar, 31750 Tronoh, Perak, Malaysia*

*Corresponding author:aaronlhe@gmail.com

Paper History

Received: 27-March-2014
Received in revised form: 7-April-2014
Accepted: 30-April-2014

ABSTRACT

The Tarpon Monopod is a minimal platform cable guyed caisson used to develop marginal fields. An in depth structural sensitivity study is performed on the Tarpon platform in 76 m water depth situated in Malaysian waters. An operating Tarpon platform offshore Peninsular Malaysia is modelled in the finite element structural analysis software, SACS v5.3 to reflect the as built condition and simulated to a combination of four different storm design criterion with two dominant approach directions to capture the monsoon seasons in the region. The guying system will be varied by simulating trivial loss of wire ropes from being intact, fully guyed to its damaged, freestanding mode. The results suggest that the Tarpon Monopod has relatively low structural redundancy and its integrity highly depends on its guying system condition. Structural weaknesses are identified alongside proposed key best practices and potential improvements to the platform.

KEY WORDS: *Tarpon Monopod; Guyed,Caisson; SACS v5.3; Finite Element; Storm Design.*

NOMENCLATURE

API	*American Petroleum Institute*
Hmax	*Maximum wave height*
Hs	*Significant wave height*
RP	*Recommended Practice*
NE	*North East*
PTS	*PETRONAS Technical Standards*
SACS	*Structural Analysis Computer System*
SW	*South West*

1.0 INTRODUCTION

More than often, smaller oil and gas fields would be deemed marginally economic, should it be developed with conventional offshore technologies like that of multi leg space frame platforms or floating systems. Such discoveries are usually left untapped until a good mix of high oil prices, innovative technologies and revamped company policies eventually justify their economic viability. The Tarpon Monopod, also known as the cable guyed caisson, is one of the many innovative minimal platform designs used in developing marginal fields.

The platform consists of a main caisson guyed with three sets of cables to anchor piles secured at the sea bed. There are currently more than 56 Tarpon platforms in use worldwide [5] with the bulk growing from a meagre 37 back in the late 90's [6]. The platform consists of a minimum topside superstructure supported on a single main structural caisson element which is guyed with three symmetrical pre tensioned cables.

Inherent in its relatively simple design and fabrication as compared to conventional jacket platforms, the Tarpon is used in developing marginal fields or fields that require a relatively quick intervention and fast tracked date to first oil or gas.

In the academia, there is a pressing need for a better understanding of the Tarpon platform in terms of its in place structural response, characteristics and sensitivity to the natural environment. For this study, due to its inherent design standardization, a single Tarpon Monopod is chosen to represent the fleet of Tarpon Monopods situated in similar water depth with matching field-topside configuration and payload.

The platform is situated in a depth of approximately 76m, offshore Terengganu in Malaysian waters [4]. It was purposefully singled out due to complete availability of supporting documents and data.

1.1 Objective of Study

Of late, there has been a need for a better understanding on the structural response and sensitivity of Tarpon monopods in Malaysian waters. The lack of specific structural inspection and maintenance procedures has bolstered this need. In the open literature, structural design documentation and studies on Tarpon platforms are very scarce and scattered. Hence, the Tarpon in place structural responses are not understood as well as conventional jacket platforms that which would put its response characteristics and sensitivity in the grey area domain of many Oil and Gas operators.

With the proliferation of marginal field developments and increase of awareness for the natural environment with millions of dollars' worth of investments at stake, this is something that should be actively avoided. Hence, this study intends to bridge the gap to shed light on the structural sensitivity of the Tarpon monopod to various design storm conditions alongside simulated damaged conditions.

1.2 Review of Tarpon Monopods

Subrata K. Chakrabarti, in the publication- Handbook of Offshore Engineering Vol.1 defined minimal platforms as fixed production platforms with a small deck used for the development of marginal fields in shallow water [3]. The minimum configurations for such platforms include typically less than ten wells, a small deck where it is possible to accommodate a coil tubing or wire line unit, a test separator and well header, a small crane, a boat landing and in some cases a minimum helideck.

Buacharoen published a study on the use of minimal platforms in the hostile waters of the Nova Scotian Offshore (NSO), eastern Canada[2]. The conclusion of this study revealed that the design of the single caisson and tripod type can be done in a way that would meet the minimal structural definitions whilst providing excellent production and structural capacity, all delivered with potential cost savings as compared to past conventional developments in the NSO region.

The tarpon monopod is a cable-guyed caisson minimal production platform. As of the year 1999, there were 37 of such platforms operating in the Gulf of Mexico, West Aftica and Indonesia. It was first used back in 1987 with StoltComex Seaway as the owner of the patents for the system. The major substructure of the Tarpon concept is made up of a central caisson, capable of housing multiple wells internally or even externally via conductor clamps. This caisson is stabilized by three cable guys at 120 degrees apart[6].

Each set of guy cables consist of two wire ropes with one end pinned to the anchor pile at or below the mud line and the other, pinned to the caisson below the water line. Generically, the anchor cables would be engineered to form a 35 degree angle from the mudline hence, giving the subsequent approximate horizontal distance of the anchor piles from the caisson to be 170 % of the water depth [6].

The major structural components of a Tarpon monopod can be listed to be: - anchor piles, structural caisson, guy cables, conductors and the topsides [8].The life cycle cost advantages of a Tarpon system are reviewed to be; low capital expenditure, simple construction, ease of installation, early production capability, low abandonment cost, recoverable and reusable components [5].

1.3 The Finite Element Model

The generic platform data used for the modelling is as tabulated in Table 1 [8].

Table 1: Generic platform data

Platform details	Data
Platform type	Monopod
Water depth	76.2m
Jacket height	82.2m
Water Depth	76.2m
Deck weight	184.8 MT
Jacket weight	800 MT
Location	Offshore Terengganu

Figure 1 is a snippet taken from the SACS Tarpon model on a 2 dimensional plane. Hence only two of the three guy cables are visible. It is obvious that the entire Topside is supported on a single main structural caisson, hence the term monopod, rather unlike the array of trusses used on a conventional fixed jacket platform.

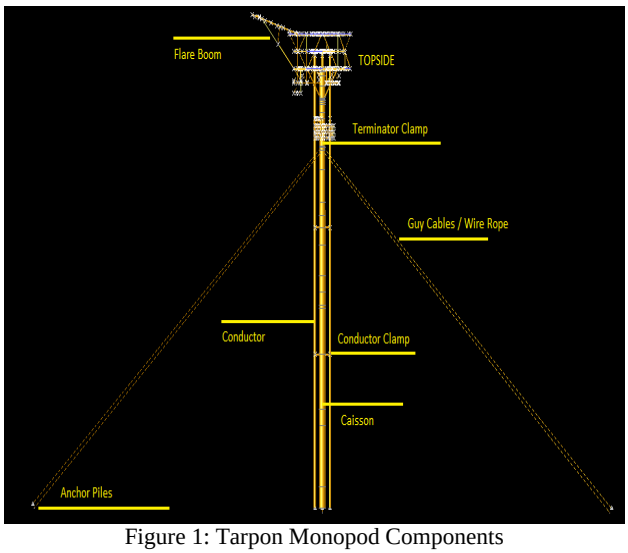

Figure 1: Tarpon Monopod Components

The main structural elements of the Tarpon Monopod are taken to be the structural caisson, wire ropes and the anchor piles. Figure 2 reports the detailed descriptions for the aforementioned structural caisson used in the model, which reflects the as built in-place condition of the platform.

Three pairs of EIPS-Independent Wire Rope Core class 6 × 61 were employed as post tensioned wire ropes. The wire ropes are attached symmetrically around the caisson to guy it to three anchor piles on the sea bed. The piling radius is approximated at 108 m from the caisson. Table 2 illustrates the key properties for the wire rope and anchor pile assembly. The structural caisson itself serves as the fourth pile with a penetration of approximately 35 m into the seabed. The in situ soil consists predominantly of clay, silt and several layers of sand.

Table 2: Wire rope - anchor pile assembly

Structural element	Description	
Wire rope	Diameter	10.16 cm
	Breaking strength	6992 kN
Anchor pile	Diameter	182.88 cm
	Wall Thickness	3.175 cm

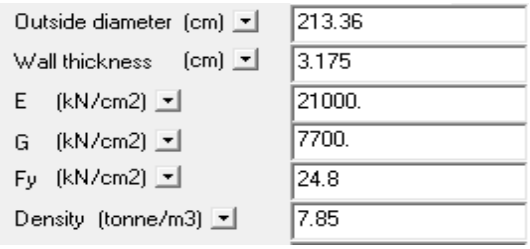

Figure 2: Structural caisson properties

A full 3-dimensional structural model showcased in Figure 3 was used for the analyses in the offshore structural analysis software, Structural Analysis Computer Software (SACS) Version 5.3. Table 3 provides a summary on the model elements and nodes.

Table 3: Finite Element Model Summary

Description	No.
Joints	938
Members	1591
Groups	54
Sections	14
Plates	174
Shell elements	0

2.0ANALYSIS METHODOLOGY

This project is broken down into three major phases. The first phase is planned as a preparatory stage which gives great emphasis on data collection and platform familiarization, alongside extensive literature reviews. The second segment would cover modelling the structural components of the platform, in place sea state, soil foundation, guy cable conditions and followed by the revised model's analysis, all performed via SACS v5.3 suite of programs.

The third phase on the interpretation of results from the latter, and presenting them in a meaningful and organized way. The supporting guidelines and codes used herein are the Petronas Technical Standard's PTS 34.19.10.30 and American Petroleum Institute's API RP 2A 21st Edition.

2.1 SACS v5.3 Analysis

SACS v5.3 Suite of Programs was used extensively for both modelling and simulation. Several SACS modules will be used herein. The first is the PRECEDE program, to be used as the graphical user modeler. The actual metocean data acquired from Offshore Engineering Centre UTP Joint Density research initiative, PETRONAS Technical Standards and the actual as designed seastate will be generated in the SACS SEASTATE module.

The Pile Soil Interaction module would be used to model the soil-pile interaction. The soil foundation data was keyed into the. The SACS IV module would be used to process and perform in place Linear static analysis coupled with nonlinear pile soil effects.

The results can then be viewed in SACS post processors such as POSTVUE which enables the results to be interpreted interactively and graphically. DYNPAC and Wave Response are employed to obtain the dynamicity of the Tarpon monopod and dynamic amplification factors to be used in the static load case analysis for incorporation of dynamic wave effects.

Tables 4~6 showcases the four different sets of storm metocean criteria, the design water depth and the Cd and Cm values respectively used in this study.

Table 4: Simulated metocean conditions

Analysis data	100 year return period		
	PTS [7]	Joint Density	As Designed [4]
Wave Height (m)	5.77 (H_s)	5.7 (H_s)	11.3 (H_{max})
Wave Period (s)	8.06	Assume 6 and 8 seconds	9.3
Current (m/s)	1.67 at surface 1.33 @ mid 0.36 @ seabed	0.69 at -3m	1.3 at surface 0.7 at seabed

Table 5: Simulated drag and mass coefficients [7]

For tubular members	Clean Member	Fouled Members
Drag Coefficient, C_d	0.65	1.05
Mass Coefficient, C_m	1.6	1.20

Table 6: Design water level computation

Description	Min	Max
Mean Sea Level, MSL(m)	76.3	76.3
Highest Astronomical Tide (m)	Not applicable	1.06
Lowest Astronomical Tide (m)	-1.13	Not applicable
Storm Surge (100 year) (m)	-	0.6
Design Water Level (m)	75.12	77.96
	Use 78m for metocean loading water level	

The storm approach is modeled from two directions to simulate the two major monsoons in Malaysian waters – The North East Monsoon and the South West Monsoon. Note that the North East monsoon has been modified at an angle to induce a certain amount of eccentricity to the storm loading on the platform. Figure 3illustrates the directionality. Marine growth used for the submerged platform members are in accordance with PTS 34.19.10.30 for the PMO region [7]. The 100 year return period wind speed used is as per the latter standard, modified by the Durst curve to 1 hour mean interval. Wind loading is then modelled as joint loads on the topside of the platform in SACS as per the recommended formula from API RP 2A [1].

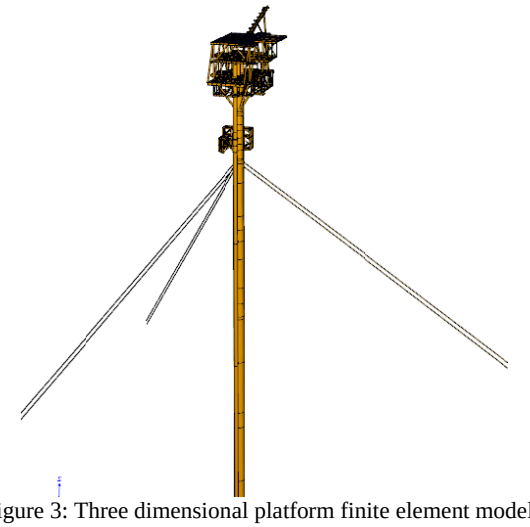

Figure 3: Three dimensional platform finite element model

The Tarpon Monopod SACS model was simulated to the array of combinations of metocean and guy system as shown in Table 7.

Table 7: Simulated scenario

No.	Metocean Data	Guyed by
1	As Designed	3 cables (intact)
	PTS	
	Joint Density(Wave T=8s)	
	Joint Density(Wave T=6s)	
2	As Designed	2 cables
	PTS	
	Joint Density(Wave T=8s)	
	Joint Density(Wave T=6s)	
3	As Designed	1 cable
	PTS	
	Joint Density(Wave T=8s)	
	Joint Density(Wave T=6s)	
4	As Designed	Free Standing
	PTS	
	Joint Density(Wave T=8s)	
	Joint Density(Wave T=6s)	
	PTS	
	Joint Density(Wave T=8s)	
	Joint Density(Wave T=6s)	

The pretension on each guy cable is simulated to 445 kN. The linear static wave loading was factored with pre-determined Dynamic Amplification Factors to be used within the in place static analysis frame in line with a quasi-static analysis methodology.

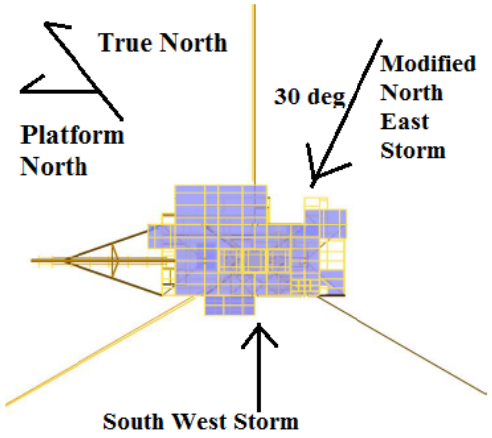

Figure 4: Storm approach direction

3.0 RESULTS

Since the Tarpon has only one main structural caisson, it is reasonable to assume that if the caisson is noted to have failed, then the Tarpon platform integrity as a whole will have been lost. Hence, a significant portion of the proceeding discussions are centered on the stiffness, dynamicity, deflections and unity check results of the single structural caisson.

It would be prudent to note here that the Tarpon model herein is located in approximately 76m water depth (MSL) and that the results published here may find application for similar Tarpon platforms situated in identical water depth and seabed condition rather than those located in shallower waters like that of the 30-50m range.

3.1 Sensitivity to loss of wire rope

As the guy cables are sequentially removed from fully guyed to freestanding a same trend can be observed for both storm approach directions. In a prevailing storm direction, the Tarpon's structural caisson experiences increasing internal loading as the guy wires are reduced.

This is an expected observation as the guy cables is inferred to provide the bulk of the Tarpon's lateral stiffness, without which the Tarpon will behave like that of a slender cylindrical cantilever beam. Table 8 shows the internal loadings at the mud line portion of the structural caisson when the platform is subjected to the worst (as designed) design storm.A comparison of stiffness values revealed dramatic loss of structural integrity from intact fully guyed to the freestanding condition. The Tarpon Monopod studied is hence unsuitable. The result summary for stiffness computation is summarized in Figures 5~6 and Table 9.

Table 8: Caisson mudline internal forces

Modified NE Storm Approach			
	Freestanding	x 1 wire	Fully guyed (x 3)
Axial (kN)	4127.9	4653.7	5364.3
Shear (kN)	1767.5	710.2	250.1
Bending (kN.m)	106000	28518.2	5828.1
South West Storm Approach			
Axial (kN)	3330.9	6982.9	5872.3
Shear (kN)	5589.8	1371.7	241.0
Bending (kN.m)	65933.6	78831.7	6605.8

Table 9: Global lateral stiffness summary

Condition	Stiffness (kN/m)
Freestanding	92.3
Intact	2357.7

It is evident from Table 9 that the Tarpon Monopod experiences a dramatic loss of stiffness in the event of full guy wire failure. The platform's dynamicity in terms of natural period also shows an obvious shift from the fixed regime to a more compliant regime, that which it is not designed for. The freestanding mode is hence, a non-real dynamic solution as the platform has failed.

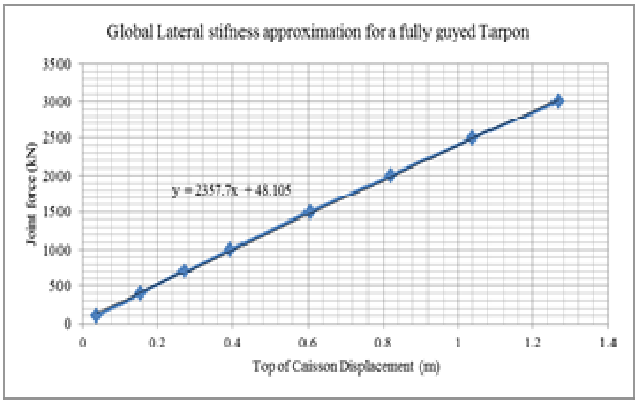

Figure 5: Global lateral stiffness for intact condition

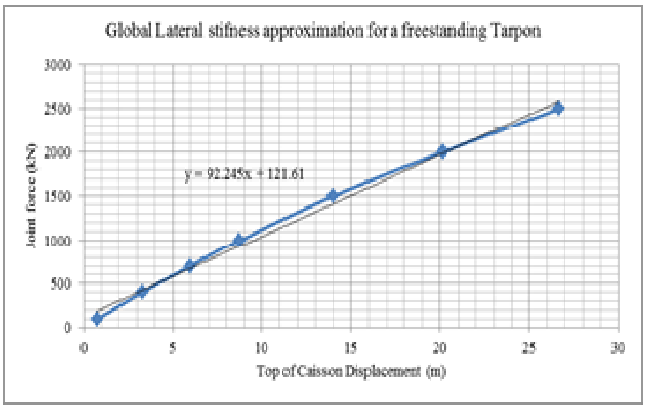

Figure 6: Global lateral stiffness for freestanding condition

3.2 Dynamic Analysis

The natural periods of the Tarpon structure were simulated via SACS DYNPAC module. In order to account for the nonlinear pile soil interaction, the foundation elements were linearized in the form of pile superelements. The dynamic mass system was selected as consistent and continuous mass. The first three modes of natural vibration are displayed in Table 10.

Table 10: First three platform natural periods

Modes	Freestanding	1 wire	2 wires	3 wires
1	16.430 s	11.224 s	3.746 s	2.418 s
2	11.847 s	2.805 s	2.403 s	2.354 s
3	2.606 s	2.377 s	2.358 s	2.344 s

3.3 Platform Deflection and Unity Check

The results from the unity checks are superimposed with the Tarpon's in place deflection as tabulated in Tables 11~12. The deflection herein is defined not as the structural caisson's displacement but as the maximum displacement experienced by a point on the Tarpon platform, usually at the topsides or flare boom.

Table 11: Caisson deflection-unity check for SW approach

Guy wire	Metocean for SW approach	Max Caisson Deflection (cm)	Max Caisson Unity Check
x 0	As Designed	13016.8	7.65
	PTS	684.6	2.79
	Joint Density 8sec	284.1	1.28
	Joint Density 6sec	348.3	1.51
x 1	As Designed	1135.4	4.4
	PTS	557.9	2.46
	Joint Density 8sec	222.5	1.11
	Joint Density 6sec	238.5	1.17
x 2	As Designed	62.1	0.55
	PTS	13.1	0.44
	Joint Density 8sec	11.2	0.35
	Joint Density 6sec	9.1	0.35
x 3	As Designed	62.1	0.55
	PTS	16.4	0.3
	Joint Density 8sec	8.1	0.24
	Joint Density 6sec	10.3	0.24

It is obvious here that the freestanding modes have all failed indefinitely. The singly guyed condition also fails under the extreme As Designed metocean criteria and marginally survives with its plastic reserve strength, when loaded with the PTS metocean criteria while it comfortably survives the joint densities.

It would be prudent to note that the guy cables will not fail in axial tension, given their high breaking strength. This is proven via a pushover analysis. At platform failure, the guy cables still possess relatively large reserve strength and do not initiate the failure sequence.

It is keenly noted that the approach of defining complete platform failure at the failure of the structural caisson is intrinsic in the nature of a caisson monotower.

Table 12: Caisson deflection-unity check for NE approach

Guy wire	Metocean for NE approach	Max Caisson Deflection (cm)	Max Caisson Unity Check
x 0	As Designed	1800.6	6
	PTS	578.3	2.46
	Joint Density 8 sec	232.9	1.12
	Joint Density 6 sec	291.8	1.34
x 1	As Designed	315.2	1.66
	PTS	179.8	1.04
	Joint Density 8 sec	82.2	0.54
	Joint Density 6 sec	91.5	0.59
x 2	As Designed	46.6	0.48
	PTS	11.0	0.29
	Joint Density 8 sec	14.2	0.23
	Joint Density 6 sec	12.9	0.23
x 3	As Designed	46.6	0.48
	PTS	15.5	0.31
	Joint Density 8 sec	7.1	0.24
	Joint Density 6 sec	9.2	0.24

3.4 Soil Sensitivity

A soil sensitivity study was performed under two foundation conditions. The intact soil condition was modelled in accordance to the soil investigation report. The degraded soil conditions were modelled to a one third reduction in shear strength for all soil strata with additional skin friction reduction for sand layers. The density for clay was reduced by one third whilst the density for sand and silt was reduced by half.

The soil sensitivity studies show that the platform's in place response is relatively insensitive to the soil condition in its intact condition. Figure 7 illustrates this. However, in damaged scenario such as a combination of maximum storm loading coupled with loss of wire ropes, the platform exhibits greater dependency on the foundation condition.

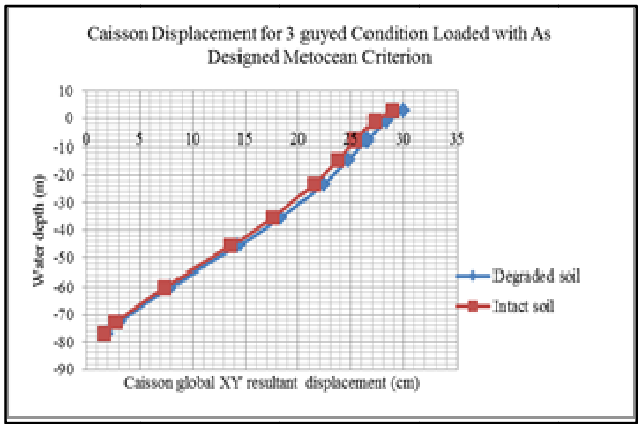

Figure 7: Intact Tarpon insensitivity to soi condition

3.5 Discussion

Like in the Modified NE direction, the SW storm approach induces failure in all freestanding Tarpons. The singly guyed Tarpon in the SW approach fails indefinitely for As designed and PTS metocean criterion The Tarpon banks on its reserve plastic strength to marginally survive the joint density storms on plastic reserve strength. For both storm directions, in intact condition, the Tarpon Monopod exhibited the largest unity check at the cable termination point on the main structural caisson. This is unlike the other conditions where the unity check was recorded maximum at the caisson mud line.

It can be well inferred here that the Tarpon monopod does not stand a storm survival chance in its freestanding mode. It is simply not designed to be unguyed. The Tarpon can also be seen to have increasing sensitivity to the direction of the storm attack as its guy cables are removed one set at a time. In its fully guyed mode, the Tarpon does not respond very differently for both monsoon storm approaches besides surviving through all simulated storm conditions.

However when the guy cables are removed sequentially, it becomes exceedingly clear on how the Tarpon's sensitivity on storm direction and magnitude increases whilst putting huge uncertainties into the picture of its integrity and robustness. For example, it can be seen that the Tarpon monopod may comfortably survive with only 1 set of cables remaining in a storm of magnitude equal to the join densities metocean criterion during a prevailing North East monsoon.

This is not the case for the Southwest storm approach where the Tarpon's structural state would have meant imminent failure for the same metocean loading. The deflections for both cases are also very different from each other. This is one of many instances where the Tarpon monopod becomes increasingly sensitive to the incoming storm direction and its integrity depends on the probability that favorable conditions would prevail, should the cable damage go unnoticed.

One of the interesting implications of these findings is that the event of a cable loss may go virtually unnoticed by topside maintenance personnel as reflected in the theoretically equal deflection magnitudes for the doubly guyed and fully guyed caisson, given that the wave, wind and current approach direction is conducive to utilize the tension capacities of the two remaining cables. This calls for an appropriate Tarpon specific inspection and maintenance regime that will be different than that of conventional jacket platforms.

3.6 Way Forward

It is obvious from this study that the Tarpon Monopod is not the most robust available option for 70-80m water depth offshore marginal field exploitations. Whilst competitive in the minimal platform market, below are some of the finer points for further improvements to the Tarpon structure that the engineer can incorporate for future developments.

- Increase in structural redundancy can be achieved by increasing the stiffness of the structural caisson, say by provision of grout to a certain length, the insertion of ring stiffeners or simply a caisson section with higher/tougher cross sectional properties.
- Improve pile capacity as to avoid plasticity. This involves considering different pile technologies such as steel hybrid – concrete grouted piles or suction piles, instead of conventional hollow steel piles.
- Form a dedicated inspection and maintenance system for the Tarpon platform.
- Consider the use of alternative marginal field platform designs. This may include but are not limited to the likes of minimal gravity based platforms where the seabed

conditions permit, mini Tension leg platform and other types of monotowers.
- Place simple axial strain/stress monitoring gauges on each guy cables to effectively observe as to how the tension in each cables fair alongside its pre-tension of 100 kips.

4.0 CONCLUSION

This study delivers a comprehensive report detailing the structural response of the Tarpon Monopod when subjected to different metocean and guying system conditions. The topline summary of the findings is as summarized below.

- The Tarpon Monopod is a structure whose integrity is highly dependent on its guying system. The lateral restraint lies primarily on its wire ropes. The main caisson merely serves as a vertical column for the placement of the topside.
- Even one set of missing guy cable may initiate structural failure during unfavorable storm approach directions.
- Its damaged condition (removed guy wires) response is vastly sensitive to different storm directions as compared to its relatively insensitive intact condition.
- It may survive with only two or even one guy wire pair given that the storm approach is favorable for utilizing the full capabilities of the remaining cables.
- In its freestanding mode, the Tarpon structure fails in all simulated storm conditions in this study.
- Attention to be given at the cable terminators and cable-pile connections.

ACKNOWLEDGEMENTS

The authors would like to thank PETRONAS for their support throughout the course of this study. To the engineers at the Offshore Engineering Centre of Universiti Teknologi PETRONAS, thank you for such reliable technical input and advice where it was needed.

REFERENCES

1. American Petroleum Institute API (2000). *Recommended Practice for Planning, Designing and Constructing Fixed Offshore Platforms - Working Stress Design*, 21st Edition. API
2. Buachareon, J. (2010). *Cost and Practical Based Concept for Innovative Design of Minimum Offshore Structures* (Master's Thesis). Thailand: School of Engineering and Technology, Asian Institute of Technology.
3. Chakrabarti, S. K. (2005). *Handbook of Offshore Engineering Vol.1*. Offshore Structure Inc. Illinois, USA: Elsevier.
4. ECL. (2008). *Detailed Engineering Design of Substructure for LEDP-A Guyed Caisson* (Substructure Design Manual).
5. LLC, T. S. (2012). *Tarpon Systems - Making Marginal Field Production More Profitable than Ever*. Retrieved 2013, from http://tarponsystems.com/pdf/Tarpon2page2NoAdd.pdf
6. Offshore (1999). *Tarpon Monotower Develops further from 37 Field Applications*. Retrieved 2013, from http://www.offshore-mag.com/articles/print/volume-59/issue-4/news/general-interest/tarpon-monotower-develops-further-from-37-field-applications.html
7. PETRONAS. (2010). *PETRONAS Technical Standards - PTS 34.19.10.30*. Malaysia.
8. Samsudin, M. S. (2012). *Structural Sensitivty and Parameter of Tarpon Platform* (unpublished dissertation). Perak, Malaysia: Universiti Teknologi PETRONAS.

Journal of Ocean, Mechanical and Aerospace
-Science and Engineering-, Vol.7

May 20, 2014

Review on Aerodynamic Characteristics of Helicopter Tail Rotor Propeller Using Quasi-Continuous Vortex Lattice Method

Firdaus,[a], Jaswar Koto,[a,b,*], M.S Ammoo, [a], I.S.Ishak,[a] and Nofrizal,[b]

[a)]*Department of Aeronautical, Automotive and Ocean Engineering, Faculty of Mechanical Engineering, Universiti Teknologi Malaysia*
[b)]*Ocean and Aerospace Research Institute, Indonesia*

*Corresponding author: mshariff@fkm.utm.my and shah@mail.fkm.utm.my

Paper History

Received: 15-January-2014
Received in revised form: 30-January-2014
Accepted: 15-May-2014

ABSTRACT

This paper reviews on application of quasi continuous vortex lattice method for determining the performance of helicopter tail rotor propeller. Tail rotor blade for Bell B206 of one seat helicopter is used. The method is developed to be suitable for analyzing the performance of propeller in term of thrust, torque, and efficiency. These parameters are calculated based on pressure on blade.

KEY WORDS:*Helicopter Tail Rotor Propeller, Quasi Continuous Vortex Lattice Method, Bell B206*.

NOMENCLATURE

VLM	Vortex Lattice Method
MFM	Mode Function Method
QCM	Quasi Continuous Method
SSPM	Simple Surface Panel Method
CFD	Computational Fluid Dynamic
LE	Leading Edge
TE	Trailing Edge

1.0 INTRODUCTION

The propeller is the device that mainly used as propulsive for marine vehicles, airplanes and rotorcraft. As it is a crucial part, it has to be designed to meet power requirement at the indicated speed with optimum efficiency. Now days, with growing demands for of higher speed and greater power, the propeller is becoming increasingly larger in size and its geometry shape become more complicated. Due this complicated geometry, the propeller should be optimally designed for increased propulsion efficiency.

To predict the steady and unsteady propeller characteristics, many numerical models and propeller theories were proposed. One of them and will be used in this study is based on lifting surface theory. The lifting surface theory also plays as important role in the hydrodynamics analysis of marine propeller. The theory has been developed for a long time in the field of aeronautics. While almost all of the applications of the theory are to wings of airplanes, there is an old application to screw propellers (Kondo, 1942).

A number of methods based on lifting surface theory to estimate the propeller characteristics have been published. They can be classified into two groups. One group is based on the continuous loading method such as Mode Function Method (MFM) and the other the discrete loading method such as Vortex Lattice Method (VLM). Due to the complexity in numerical calculation using MFM, its application to unconventional propellers is not easy. VLM, however, also has some room to be

improved; in the neighborhood of leading edge, vortex strength predicted by VLM is always lower compared with analytical solutions. Owing to the discrete and concentrated loading distribution, pressure distribution is not estimated straightforwardly. Leading edge suction force is not estimated straightforwardly either. A large number of elements are necessary to get converged solutions (Naoto Nakamura, 1985).

Taking the above circumstances into consideration, a numerical method to estimate aerodynamics characteristics of helicopter tail propeller based on Quasi-Continuous Method (QCM) will be developed. QCM has both advantages of continuous loading method and discrete loading method; loading distribution is assumed to be continuous in chord-wise direction and stepwise constant in span-wise direction. Simplicity and flexibility of discrete loading method are also retained.

2.0 LITERATURE REVIEW

2.1 Quasi Continuous Method Theory

C. Edward LAN (1974) has developed a quasi-continuous method for solving the thin wing problem. In his study, the spanwise vortex distribution is assumed to be stepwise constant while the chordwise vortex integral is reduced to a finite sum through a modified trapezoidal rule and the theory of Chebychev polynomials, in order to satisfying the boundary condition. Wing edge and Cauchy singularities are accounted for, based on two-dimensional theory; that contain the conventional Vortex Lattice Method and the present analysis. Based on his conclusions, the wing square-root singularities and the Cauchy singularity has been properly accounted for in this method, compared to the conventional vortex lattice method. The total aerodynamic characteristics are obtained by an appropriate quadrature integration. The two-dimensional results for airfoil without flap deflection reproduce the exact solutions in lift and pitching moment coefficients, the leading edge suction, and the pressure difference at a finite number of points. For a flapped airfoil, the present results are more accurate than those given by the vortex lattice method. The three dimensional results also show an improvement over the results of the vortex lattice method.

Naoto Nakamura (1985) has conducted research on estimation of propeller open- water characteristics base on Quasi – Continuous Method. This study show that comparisons of propeller open-water calculated by this method with measured data showed good agreement for a wide variety of propellers. This method is promising for the improvement of numerical methods in propeller lifting surface theory. However, for propeller with extremely large skew, the estimation accuracy was not so good. Nakamura recommended for improvement, a more realistic wake model should be formulated based on the geometry of slipstream such as contraction, variation of pitch etc. Force acting on source distribution and leading edge suction force should properly accounted for. And lastly, more exact treatment of blade thickness is necessary for the improvement in the calculation accuracy of pressure distribution on blade surface.

J.Ando and KuniharuNakatake (1999) have conducted a calculation method for the three – dimensional unsteady sheet cavitation hydrofoil problem. This method is based on simple surface panel method “SQCM” which satisfied easily the Kutta condition even in the unsteady condition problem. This method uses source distribution (Hess and Smith, 1964) on the hydrofoil surface and discrete vortex distribution arranged on the mean chamber surface according to QCM (Quasi-Continuous vortex lattice Method) (Lan, 1974). These singularities should satisfied the boundary condition that the normal velocity is zero on the hydrofoil and the mean camber surface. The partially cavitation hydrofoil was treated in heaving motion and both partially cavitation and super cavitation was in sinusoidal gust. The calculated results ware compared with other calculated results and the accuracy of the present result is confirmed.

J. Ando and K. Nakatake (2000) have conducted research on a new surface panel method to predict steady and unsteady characteristic of marine propeller. These methods represent the flow field around a wing by the source and the doublet distributions on the wing surface, and are applied successfully to calculation of the pressure distribution on the propeller blade. But it is not easy to satisfy the Kutta condition at the tailing edge and many discussions were raised about it (Koyama, 1989). A reasonable expression of the Kutta condition is that the pressure becomes equal on the upper and lower wing surfaces at the tailing edge. In order to satisfy the above condition, it is need to solve iteratively the quadratics simultaneous equations for singularity distributions. They have developed a new surface panel method which is a kind of singularity method. This method uses source distributions (Hess and Smith, 1964) on the wing surface and discrete vortex distribution arranged on the chamber surface according to quasi-continuous method vortex lattice method (QCM) (Lan,1974). Then these singularities both the wing surface and the camber surface condition that the normal velocity should be zero in case of the steady problem. Since these singularities satisfy automatically Kutta condition, they not need use any iterative procedure. In case of the unsteady problem, they introduce the normal velocity to the chamber surface at the trailing edge in order to make the pressure difference between the upper and the lower wing surface zero. Even though the iterative procedure to satisfy the Kutta condition is necessary, the convergence is quite fast. They named this simple surface panel method SQCM (source and QCM). In SQCM, the upper and the lower surface of the propeller blades are divided into the same numbers of source panels, respectively. Then the ring vortices are located on the mean chamber according to the unsteady QCM (Hoshino, 1985) (Murakami et al., 1992). The hub surface is also divide into source panels. The trailing vortices flow out as ring vortices from the trailing edge every time step. They assume that

the trailing vortices leave the trailing edge in tangential to the mean chamber surface and the pitch of trailing edge vortices reach an ultimate value, which is the mean of geometrical pitch distribution of the propeller blade, within a haft revolution. They solved the boundary conditions every time step Δt. The source distributions on propeller blades and hub surface and the vortex distributions on the chamber surface are obtained for each time step from the boundary conditions at the center of the source panels and control points on chamber surfaces whose positions are determined by the QCM theory. Here the pressure Kutta condition is considered simultaneously. The perturbation potentials and velocity distributions on the blade surfaces are obtained from the singularity distributions. The pressure distributions are calculated by the unsteady Bernoulli's equation. Then the force acting on propeller blades are obtained by pressure integration on the propeller blade.

J.Ando (2009) has done the numerical analysis of steady and unsteady sheet cavitation on a marine propeller using a Simple Surface Panel Method (SSPM). This SSSPM uses source distribution on propeller blade surface from Hess & Smith (1964) and discrete vortex distributions arranged on the camber surface according to QCM (Quasi-Continuous vortex lattice Method) by Lan (1974). The singularities satisfy the boundary condition that the normal velocity is zero on the propeller blade and mean chamber surface. From this analysis Jun Ando concluded that present method can predict the thrust and the torque in extensive advance coefficients and cavitation numbers. For unsteady case, this method can express the variations of the cavity area and cavity volume. And the cross flow effect on the cavity surface gives reasonable cavity shapes and variations of cavity area and volume especially in HSP.

2.2 Lifting Surface Theory

Research on application of the lifting surface theory to marine propeller was carried out by Koichi Koyama (2012). In this research they use three methods, named here Method 1, Method 2, and Method 3, of propeller lifting surface theory proposed by Hanoaka (1969). Method 1 and Method 3 in this research belong to mode function method group, and Method 2 belongs to discrete function method group. Method 1 may be called series expansion method. Two – dimensional integral equation for lifting surface is converted into simultaneous one-dimensional integral equations, in expanding the two-variable integral equation in power series of one- variable by Taylor' theorem and equating the coefficient functions of successive powers to zero. The method is equivalent to Flax's method on condition that the mode function is orthogonal series. The method, however, is distinguished by easy calculation of coefficients of simultaneous equations in comparison with Flax's method. The method can deal with the simple mean chamber line accurately without many chordwise control points in contrast to the collocation method. The method reduces the labour for numerical integration along the helical surface to the minimum. Especially for the case of unsteady condition, the machine running time for calculation not long. In Method 2, existing integral equation is solved by the doublet-lattice method. The blade is divide into many blade element by cylindrical surface, and each blade element is divided into many boxes. Surface distribution of doublet in the pressure field is replaced by line doublets with constant strength and direction in every box. The chordwise arrangement is determined by Lan's method, which is devised so as to give the accurate solution near the leading edge. Method 1 yields valid circulation density in wide range near the tip and yields valid circulation of blade section in all range for the usual broad bladed propeller. The method is useful for the calculation of propeller forces. Method 2 gives the converged chordwise distribution of circulation density. It is supposed to give the accurate solution near the leading edge and to be useful for the calculation cavitation. Method 3 yield the accurate solutions for the circulation density near the blade tip as well, even though the blades are highly broad. The method is considered useful for the calculation of cavitation. There are many possibilities of application of the propeller lifting surface theory to the propeller design. The following are some examples of the application method to be employed in the design procedure. The blade outline is adjusted according to the inflow variation of hull wake from the view point of vibratory propeller forces, when Method 1 is useful. If the blade outline is given, the relation between upwash and loading is controlled by the lifting surface theory. If the pitch of the helical surface is assumed to fix, single calculation of the matrix of coefficient corresponding to the integral equation, make it possible to obtain upwash distribution and to obtain loading distribution by the upwash distribution with ease. In this case, Method 2 and Method 3can control accurately the pitch correction or chamber correction in the design method, from the cavitation point of view.

Koichi Koyama (2012) has conducted relation between the lifting surface theory and the lifting line theory in the design of an optimum screw propeller. This research is based on the propeller lifting surface theory. Circulation density (lift density) of the blade is determined by the lifting surface theory on a specified condition in general. However, it is shown that, in the case of optimum condition, the circulation density is not determined by the lifting surface theory, although the circulation distribution which is the chordwise integral of the circulation density is determined. The reason is that the governing equation of the optimization by the lifting surface theory is reduced to that by the lifting line theory.

2.3Propeller

Davide Grassi has done numerical for analysis of the dynamics characteristics propeller in uniform and stationary inflow by lifting surface theory where this lifting surface analysis method based upon Kerwin (1978) theory. These procedures employs a simplified defined shape for representing propeller wake

geometry which given good results for moderately skewed blade geometries not too far from their design point, while tend to overestimate thrust and torque at low advance coefficient. To overcome this difficulties, DavideGrassi was employed this analysis fully numerical wake adaption method. The present tool employs a discrete vortex line representation of the blade, with elements located at the exact mean surface. The leading edge suction and tip vortex separation was consider in an accurate and efficient way. The propeller was assumed to work in an inflow with radially varying axial and tangential component, while the presents of the hull hub and free surface is discounted. The blade force calculation was separated into three components, force acting on vortex sheet elements that determined by using Kutta – Joukowski theorem, force acting on source singularity determined by using Lagally's theorem, and viscous drag forces are calculated at each radial position using a global frictional coefficient experimentally. Tip separation effect has been considered based on the Kerwin's formulation. These segment with the local velocity vector is necessary to align, since chordwise vortex element are to be force free. Vortex ring corner points placed at bladed tip are all shifted in a direction normal to the mean surface by a quality linearly proportional to its position on the tip chord. The effect of tip vortex separation is in the logically to increase propeller thrust and torque at low advance coefficient, while its effect is negligible around the design advance coefficient.

A. Brocklehurst (2012) has make the review of helicopter tip shapes to discussed the evolution of helicopter blade designs and tip shapes, and the development of methods for their analysis and evaluation. The review has identified three main types of helicopter tip designs: the parabolic tip, the swept (tapered) tip, and the BERP tip. In addition there are several tip shapes intended to alleviate BVI noise by splitting, or diffusing the tip vortex. The literature review has identified some overlap with fixed-wing aircraft, particularly with regard to tip aerodynamics and the details of vortex formation. While there are some obvious fundamental differences, both fixed-wing and rotary-wing con-figurations require accurate resolution of the flow-field if the results are to be useful in tip design studies. The nature of the helicopter problem is, however, much more complex than fixed-wing and is much more demanding from a modelling point of view due to the need to preserve wake vortices, take into account variations in incidence and sideslip (in cruising flight), and also include unsteady effects. The design must also work within much tighter moment constraints. Nevertheless, much can be learnt from validating the methods against fixed-wing tests, and there is considerable carry-over in some of the detailed design thinking. In particular, the work of Hoerner and K¨uchemann has provided a basis for generating improved tip shapes. The review has also covered the development of computational methods. Analysis techniques have developed from rotor models based on lifting-line and lifting-surface theory, with a prescribed or free wake, to the application of sophisticated CFD methods. Initially the numerical approach required some of the world's largest computers, but these modern methods are now becoming available in industry, and offer greater insight and higher resolution than traditional design methods. Two main features of the computational approach would appear to require further development for helicopter applications. One is that it is important to fully capture the wake in order to determine the correct flow-field around the rotor blade, and the other is that the solver needs to include boundary layer transition in both steady and unsteady (3D) conditions, if accurate overall performance and the effects of retreating blade stall are to be predicted. Much effort has been expended on coupling wake models with near-field Navier–Stokes solutions in an effort to obtain the desired accuracy at acceptable computational cost. It is also clear that rotor trim and blade deflections are important aspects of helicopter simulation. Often, the rotating and pitching blades may operate in proximity to a stationary fuselage, or fin, and this presents challenges in grid generation, requiring the use of sliding grids, or Chimera overset grid techniques. From the literature there appears to be a preference toward structured grids to resolve the flow features, but some developers favor the Chimera approach. It is also clear that CFD methods are maturing quickly and through rapidly growing computer resources will soon be universally accepted and indispensable for rotor blade design evaluations. Recent research effort on CFD has been directed towards tackling the challenging problems of whole helicopter simulations. Coupling of CFD with structural dynamics to take into account blade deflections has also been a focus of attention, and offers to greatly improve the fidelity of the simulation. Most recently, fast harmonic-balance methods have begun to emerge which promise further run-time reductions for forward flight simulations. However, while CFD has been applied to a range of rotors problems, including investigations of tilt-rotors, little new work has been found on the use of CFD for the design of new tip shapes, particularly for tail rotors.

3.0 HELICOPTER DESIGN PROBLEM

One of the very first problems helicopter designers encountered when they tried to create a machine that could hover was the problem of torque reaction (Guo-HuaXu, 2001). Newton's third law of motion requires that for every action there is an equal and opposite action. A typical single main rotor helicopter has a rotor system mounted on a rotor mast. The helicopter engine supplies power so that the helicopter can turn the mast, and thus the rotor system connected to it. When the helicopter applies torque to the mast to spin it, there is an equal-and-opposite torque reaction which tries to turn the helicopter in the opposite direction as shown in Figure 1.

Igor Sikorsky seems to be the first to settle on using a single

rotor mounted at the rear of the helicopter as a way to counter the torque. This is the most popular arrangement today. Sikorsky actually experimented with many different arrangements before selecting a single tail mounted rotor. It seems strange that the majority of helicopters produced use this method of countering torque, given that there are several major problems with this method which are not encountered with counter-rotating rotor systems (J. Gordon Leishman, 2002).

One major problem with tail rotors is that they rob an enormous amount of power. As a rule of thumb, tail rotors consume up to 30% of the engine power (C. Young, 1976).Still another problem with tail rotors is that they are fairly difficult to control accurately. Turbulence and crosswinds make it extremely difficult to hold a constant heading in a tail rotor equipped helicopter. The workload is very high, and good results are difficult to achieve. Many larger helicopters end up being designed with a yaw stabilization system, which is essentially an autopilot for the tail rotor.In the study, one seat helicopter is used as a case study as shown in Figure.2

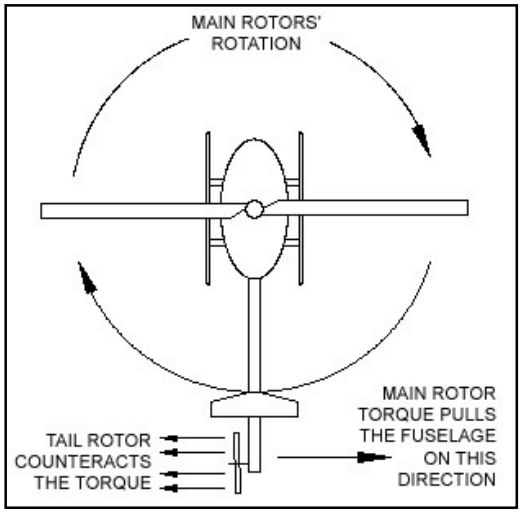

Figure 1: Tail rotor function

Figure.2: One seat helicopter.

4.0 TAIL HELICOPTER ROTOR BLADE

In this study, offsets coordinate from tail rotor blade for Bell B206 helicopter will be used as simulation data to calculate the air forces and other performance characteristics on the rotor blade as shown in Fig.3-4. Experimental will be done to make comparison with the data from simulation to ensure that data will be valid for both simulation and experimental.

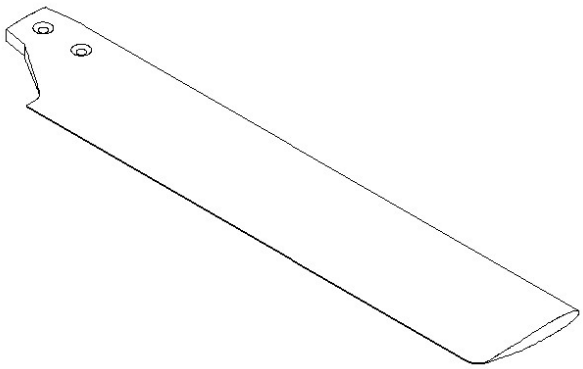

Figure 3: The real model of tail rotor blade for Bell B206.

Figure 4: Tail propeller blade of helicopter.

5.0 CALCULATION METHOD

5.1 Outline of Quasi-Continuous Vortex Lattice Method

The propeller blade is divided into M panels in the spanwise direction. The face and back surfaces of the blade section are divide into N panels in the chordwise direction, respectively. Therefore, the total number of source panels becomes *(M × 2N) × K* and constant m is distributed in each panel. The total *(M × 2N) × K* horse shoe vortices are located on the mean chamber surface according to Eq. 1 as illustrated in Figure 5.

$$\xi_{\mu\nu}^{\mathrm{LP}} = \xi_{\mathrm{L}}(\mathrm{r}_{\mu}) + \frac{\xi_{\mathrm{T}}(\mathrm{r}_{\mu})-\xi_{\mathrm{L}}(\mathrm{r}_{\mu})}{2}\left(1 - cos\frac{2\nu-1}{2\mathrm{N}_{\gamma}}\pi\right) \quad (1)$$

$$\xi_{\mu\nu}^{\mathrm{CP}} = \xi_{\mathrm{L}}(\bar{\mathrm{r}}_{\mu}) + \frac{\xi_{\mathrm{T}}(\bar{\mathrm{r}}_{\mu} - \xi_{\mathrm{L}}(\bar{\mathrm{r}}_{\mu})}{2}\left(1 - cos\frac{\nu}{2\mathrm{N}_{\gamma}}\pi\right)$$

where,

$$\bar{\mathrm{r}}_{\mu} = \frac{1}{2}(\mathrm{r}_{\mu} + \mathrm{r}_{\mu+1}) \quad (2)$$

μ and ν are numbers in the spanwise and chordwise directions. $\xi_{\mathrm{L}}(\mathrm{r}_{\mu})$ and $\xi_{\mathrm{T}}(\mathrm{r}_{\mu})$ are the positions of the leading edge and trailing edge, respectively.

The induced velocity vector due to ν-th ring vortex of unit strength which start from the μ-th strip and ones due to the ℓ-th ring vortex of unit strength located in trailing wake defined as $\vec{v}_{k\mu\nu}^{\gamma}$ and $\vec{v}_{k\mu\ell}^{w}$. These induced velocity vectors are expressed as

$$\vec{\mathrm{v}}_{\mathrm{k}\mu\nu}^{\gamma} = \vec{\mathrm{v}}_{\mathrm{k}\mu\nu}^{\mathrm{B}} + \sum_{\nu=\nu}^{\mathrm{N}_{\gamma}}(\vec{\mathrm{v}}_{\mathrm{k}\mu+1\acute{\nu}}^{\mathrm{F}} - \vec{\mathrm{v}}_{\mathrm{k}\mu\acute{\nu}}^{\mathrm{F}}) - \vec{\mathrm{v}}_{\mathrm{k}\mu\ell}^{\mathrm{ws}}|_{\ell=1} \quad (3)$$

$$\vec{\mathrm{v}}_{\mathrm{k}\mu\ell}^{\mathrm{w}} = \vec{\mathrm{v}}_{\mathrm{k}\mu\ell}^{\mathrm{ws}} - \vec{\mathrm{v}}_{\mathrm{k}\mu\ell+1}^{\mathrm{ws}} + \vec{\mathrm{v}}_{\mathrm{k}\mu+1\ell}^{\mathrm{wc}} - \vec{\mathrm{v}}_{\mathrm{k}\mu\ell}^{\mathrm{wc}}$$

where, $\vec{v}_{k\mu\nu}^{B}$ is the induced velocity vector due to the bound vortex of unit strength on the mean camber surface, $\vec{v}_{k\mu\acute{\nu}}^{F}$ the induced velocity vector due to the free vortex of unit strength on the mean camber surface, $\vec{\mathrm{v}}_{\mathrm{k}\mu\ell}^{\mathrm{ws}}$ the induced velocity vector due to the spanwise shed vortex of unit strength in the trailing wake and $\vec{\mathrm{v}}_{\mathrm{k}\mu\ell}^{\mathrm{wc}}$ is the induced velocity vector due to the streamwise trailing vortex of unit strength in the trailing edge.

The induced velocity vector $\vec{V}$ due to each line segment of vortex is calculated by the Biot-Savart law. The segment of the ring vortex on the mean chamber surface at time t_{L} and the ring vortex in the trailing edge wake defined as $\gamma_{k\mu\nu}(t_{\mathrm{L}})$ and $\Gamma_{k\mu}(t_{\mathrm{L}})$, the induced velocity vector due to the vortex model of the QCM theory in given by the following equation.

$$\vec{V} = \sum_{k=1}^{K}\sum_{\mu=1}^{M}\sum_{\nu=1}^{N_{\gamma}}\gamma_{k\mu\nu}(t_L)\vec{\mathrm{v}}_{\mathrm{k}\mu\nu}^{\gamma}\Delta\xi_{\mathrm{L}} + \sum_{k=1}^{K}\sum_{\mu=1}^{M}\sum_{\ell=1}^{L-1}\Gamma_{k\mu}(t_{L-\ell})\vec{\mathrm{v}}_{\mathrm{k}\mu\nu}^{\gamma}\Delta\xi_{\mathrm{L}}\vec{\mathrm{v}}_{\mathrm{k}\mu\ell}^{\mathrm{w}} \quad (4)$$

where

$$\Delta\xi_{\mu\nu} = \frac{\pi c(\bar{\mathrm{r}}_{\mu})}{2N_{\gamma}}\sin\frac{2\nu-1}{2\mathrm{N}_{\gamma}}\pi, \qquad \Gamma_{k\mu}(t_L) = \sum_{\nu=1}^{N_{\gamma}}\gamma_{k\mu\nu}(t_L)\Delta\xi_{\mu\nu},$$

and $c(\bar{\mathrm{r}}_{\mu})$ is the chord length of μ section.

This Equation (4) is used when the control points are on the mean camber surface (J. Ando, 2012). When the control points are on the blade surface, the ring vortices are close to the control points especially for the thin wing. For this case, the ring vortices on the mean camber surface and shed vortex nearest to T.E. treat

as the vortex surface in order to avoid numerical error. This is called the "thin wing treatment" (S. Maita, 2000).

J. Ando and T. Kanemaru (2012) has been modify the vortex model of the QCM theory (Fig.5.b) as follows:

For first step, the ring vortex on the mean camber surface at trailing edge is closed and located the ring vortices ABCH, HCDG and GDEF downstream from trailing edge as shown in (Fig.5.b).

After that the ν-th ring vortex replace with a set of ring vortices distribution along $\Delta\xi_{\mu\nu}(\xi^{CP}_{\mu\nu-1}\sim\xi^{CP}_{\mu\nu})$ on the mean camber surface as illustrated in the middle of Fig. 5b. Then the ring vortex ABCH just downstream from trailing edge and ring vortex HCDG are replaced with a set of ring vortices distribution along $\Delta\xi^{w}_{\mu}$ in the trailing wake. The other ring vortices form $\Delta\xi^{w}_{\mu}$ are calculated as discrete ring vortices.

For this case, the induced velocity vectors due to the vortex systems on the mean camber surface and trailing wake are expressed as

$$\overrightarrow{V_\gamma} = \sum_{k=1}^{K}\sum_{\mu=1}^{M}\sum_{\nu=1}^{N_\gamma}\gamma_{k\mu\nu}(t_L)\int_{\xi^{CP}_{k\mu\nu-1}}^{\xi^{CP}_{k\mu\nu}}\vec{v}^{\gamma}_{k\mu}(\xi)d\xi + \sum_{k=1}^{K}\sum_{\mu=1}^{M}\sum_{\nu=1}^{N_\gamma}\gamma_{k\mu\nu}(t_L)\frac{\Delta\xi_{\mu\nu}}{\Delta\xi^{w}_{\mu}}\int_{\xi_T(\bar{r}_\mu)}^{\xi_T(\bar{r}_\mu)+\Delta^{w}_{\mu}}\vec{v}^{ABCH}_{k\nu}(\xi)d\xi + \sum_{k=1}^{K}\sum_{\mu=1}^{M}\Gamma_{k\mu}(t_L-1)\frac{1}{\Delta\xi^{w}_{\mu}}\int_{\xi_T(\bar{r}_\mu)}^{\xi_T(\bar{r}_\mu)+\Delta^{w}_{\mu}}\vec{v}^{HCDG}_{k\mu}(\xi)d\xi + \sum_{k=1}^{K}\sum_{\mu=1}^{M}\Gamma_{k\mu}(t_L-1)\vec{v}^{GDEF}_{k\mu} + \sum_{k=1}^{K}\sum_{\mu=1}^{M}\sum_{\ell=2}^{L-1}\Gamma_{k\mu}(t_L-\ell)\vec{v}^{w}_{k\mu\ell} \quad (5)$$

where

$$\vec{v}^{\gamma}_{k\mu\nu}(\xi) = \vec{v}^{B}_{k\mu}(\xi) + \left(\vec{v}^{F}_{k\mu+1}(\xi) - \vec{v}^{F}_{k\mu}(\xi)\right) + \sum_{\nu=\nu+1}^{N_\gamma}\left(\vec{v}^{F}_{k\mu+1\nu} - \vec{v}^{F}_{k\mu\nu}\right) - \vec{v}^{AB}_{k\mu}$$

$$\vec{v}^{ABCH}_{k\mu}(\xi) = \vec{v}^{AB}_{k\mu} + \vec{v}^{BC}_{k\mu+1}(\xi) - \vec{v}^{AH}_{k\mu}(\xi) - \vec{v}^{HC}_{k\mu}(\xi)$$

$$\vec{v}^{HCDG}_{k\mu}(\xi) = \vec{v}^{HC}_{k\mu}(\xi) + \vec{v}^{CD}_{k\mu+1}(\xi) - \vec{v}^{HG}_{k\mu}(\xi) - \vec{v}^{GD}_{k\mu}$$

$$\vec{v}^{GDEF}_{k\mu} = \vec{v}^{GD}_{k\mu} + \vec{v}^{DE}_{k\mu+1} - \vec{v}^{GF}_{k\mu} - \vec{v}^{FE}_{k\mu}$$

The velocity vector $\vec{V}$ around a propeller in the propeller-fixed coordinate system is expressed as

$$\vec{V} = \vec{V}_I + \vec{V}_\gamma + \vec{V}_m, \quad (6)$$

where $\vec{V}_I$, $\vec{V}_\gamma$ and $\vec{V}_m$ are inflow, induced velocity vectors due to vortex and source distributions, respectively.

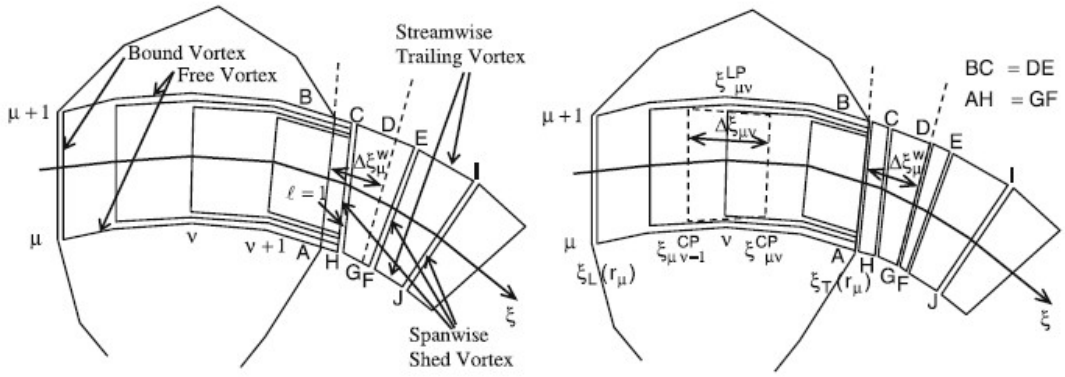

Figure 5: Arrangement of vortex system. a) From QCM. b) Thin wing treatment.

5.2 Boundary Condition and Numerical Procedure

The boundary condition of the control points on the rotor blade and mean camber are that there is no flow across the surface. But, to satisfy the Kutta condition as expressed by Equation (7), there exists at trailing edge the normal velocity which was introduced. So, the equation for the boundary condition as expressed by Equation (8).

$$\Delta p = \rho\frac{\partial}{\partial t}(\phi_+ - \phi_-) + \frac{1}{2}\rho(V_+^2 - V_-^2) \quad (7)$$

$V.n = 0$ on wing and camber surfaces (except trailing edge)

$V.n = V_N$ at trailing edge (8)

Where n is the normal vector on the blade and mean camber.

The unknown value are the vortex strength on the mean camber surface, source strength on the blade and normal velocity $\vec{V}_N$ at T.E. $\vec{V}_N$ is expressed by the following equation and determined so as to satisfy the Kutta condition iteratively.

$$V_N^{(i+1)} = \frac{\Delta p^{(i)} \beta}{\rho |V_I|} + V_N^{(i)} \tag{9}$$

where i is the number iteration. From the Equation (7), □_+ and □_- or V_- and V_+ are the mean of the magnitude or perturbation potential of the velocity at the control point on the upper and the lower surface blade, where it is close to trailing edge. This iteration is move on until Δp is small enough. According to J. Ando (2012), in this calculation $\beta = 1$ and β means the accelerations factor. In the unsteady of QCM, the Kutta condition is when $\Delta p = 0$ .The first term in the right hand side in Equation (9) means the corrector for the value of the previous step $V_N^{(i)}$ which is proportional to the pressure difference $\Delta p^{(i)}$. The iteration is continued until the pressure difference becomes small $(\Delta C_p < 0.5 \times 10^{-3})$. Assuming the normal velocity V_N at trailing edge at each iterative step, Equation (8) can be solved as the linear simultaneous equations for singularity distributions.

5.3 Unsteady Pressure and Propeller Forces

The unsteady pressure distribution on the propeller blade is calculated by the unsteady Bernoulli equation expressed as

$$p(t) - p_0 = -\frac{1}{2}\rho(|V|^2 - |V_I|^2) - \rho\frac{\partial \phi}{\partial t} \tag{10}$$

where
p_0 = the static pressure in the undisturbed inflow
p = the density of the fluid
ϕ= the perturbation potential in the propeller coordinate system
The time derivative term of ∂ in Equation (10) is obtained numerically by two points upstream difference scheme with respect to time.

The blade pressure of the propeller is expressed as the pressure coefficient C_p in order to compare the calculate results with the experimental data. The pressure coefficient is defined by

$$C_p = \frac{p(t) - p_0}{\frac{1}{2}\rho n^2 D^2} \tag{11}$$

where n is the rate of the revolutions of the propeller and D is the diameter of the propeller.

The lift, drag and moment coefficients are given by the relationships

$$C_L = \frac{L}{\frac{1}{2}\rho A V^2}, C_D = \frac{D}{\frac{1}{2}\rho A V^2}, \text{ and } C_M = \frac{M}{\frac{1}{2}\rho A l V^2} \tag{12}$$

in which A is the propeller area, l is a reference length, V is the free stream incident velocity, ρ is the density of the fluid, L and $D$are the lift and drag forces, perpendicular and parallel respectively to the incident flow, and M isthe pitching moment defined about a convenient point.

For analysis purposes, the sectional lift, drag and moment coefficients are given by the relationships

$$c_L = \frac{L}{\frac{1}{2}\rho c V^2}, c_D = \frac{D}{\frac{1}{2}\rho c V^2}, \text{ and } C_M = \frac{M}{\frac{1}{2}\rho c^2 V^2} \tag{13}$$

in which c is the section chord length and L', D' and M' are the forces and moments per unit span.

The thrust T and the torque Q of the propeller are calculated by pressure integration. Denoting the x-, y- ad z- components of the normal vector on the blade surface by n_x, n_y and n_z, respectively, the thrust and the torque are expressed by

$$T(t) = \int\int_{S_B+S_H} (p(t) - p_0) n_x ds \quad , \quad Q(t) = \int\int_{S_B+S_H} (p(t) - p_0)(n_y z - n_z y) ds \tag{14}$$

According to Naoto Nakamura (1985), in the steady calculation the viscous components of the thrust and the torque are considered approximately using the viscous drag coefficient of blade element C_d at the radius r. these component T_D and Q_D are expressed as

$$T_D = -K\frac{1}{2}\rho \int_{r_H}^{r_0} C_d(r) \bar{W}(r) \bar{V}_x(r) c(r) dr$$

$$Q_D = K\frac{1}{2}\rho \int_{r_H}^{r_0} C_d(r) \bar{W}(r) \overline{V_\theta}(r) c(r) dr$$

$$C_d(r) = \begin{cases} 0.0084 + 0.016\left(\frac{t}{c}\right) & for\ C_l < 0.2 \\ 0.0084 + 0.016\left(\frac{t}{c}\right) + 0.03(C_l - 0.2) & for\ C_l \geq 0.2 \end{cases} \tag{15}$$

where
c_l = sectional lift coefficient
$\bar{W}(r) = \sqrt{\bar{V}_x(r)^2 + \overline{V_\theta}(r)^2}$
$\bar{V}_x(r)$ = x- component of resultant flow velocity averaged in the chord wise direction
$\overline{V_\theta}(r)$ = θ- component of resultant flow velocity averaged in the chord wise direction
$c(r)$ = chord length of the rotor blade
r_0 = propeller radius
r_H = hub radius
t/c = thickness ratio

The force F_X, F_Y, F_Z and moments M_X, M_Y, M_Z is acting on the propeller in the X, Y, Z directions of the space coordinate system are expressed as

$$F_X(t) = -T(t) = \int\int_{S_B+S_H} (p(t) - p_0) n_x ds$$

$$F_Y(t) = \int\int_{S_B+S_H} (p(t)-p_0)(n_y\cos(\Omega t) + n_Z\sin(\Omega t))\ ds$$

$$F_Z(t) = \int\int_{S_B+S_H} (p(t)-p_0)(n_z\cos(\Omega t) - n_y\sin(\Omega t))\ ds$$

$$M_X(t) = Q(t) = -\int\int_{S_B+S_H} (p(t)-p_0)(n_y z - n_z y)ds$$

$$M_y(t) = -\int\int_{S_B+S_H} (p(t)-p_0)[(n_z x - n_x z)\cos(\Omega t) + [(n_x y - n_y x)\sin(\Omega t)]ds$$

$$M_z(t) = -\int\int_{S_B+S_H} (p(t)-p_0)[(n_x y - n_y x)\cos(\Omega t) + [(n_x z - n_z x)\sin(\Omega t)]ds \quad (15)$$

For the force and moments are nondimensionalized as below:

$$K_{FX}(t) = \frac{F_X(t)}{\rho n^2 D^4} \quad , \quad K_{FY}(t) = \frac{F_Y(t)}{\rho n^2 D^4}$$

$$K_{FZ}(t) = \frac{F_Z(t)}{\rho n^2 D^4} \quad , \quad K_{MX}(t) = \frac{M_X(t)}{\rho n^2 D^5}$$

$$K_{MY}(t) = \frac{M_Y(t)}{\rho n^2 D^5} \quad , \quad M_{MZ}(t) = \frac{M_Z(t)}{\rho n^2 D^5} \quad (16)$$

Finally the advance J, the torque and the thrust coefficientK_Q, K_T and the propeller efficiency η_p are expressed as follows:

$$J = \frac{V_A}{nD} \quad , \quad K_T = \frac{T}{\rho n^2 D^4}$$

$$K_Q = \frac{Q}{\rho n^2 D^5} \quad , \quad \eta_p = \frac{J}{2\pi}\frac{K_T}{K_Q} \quad (17)$$

6.0 CONCLUSION

In conclusion, this paper reviewed on prediction of performance of helicopter tail propeller using quasi continuous vortex lattice method. As a case study, tail rotor blade for Bell B206 for one seat helicopter is used. The performance of the propeller is analyzed in terms of thrust, torque and efficiency.

REFERENCE

1. C. Edward Lan. 1974. A Quasi-Vortex-Lattice Method in Thin Wing Theory. The University of Kansas, Lawrence, Kan.
2. Naoto Nakamura. 1985. *Estimation of Propeller Open-Water Characteristics Based on Quasi-Continuous Method*. Spring Meeting of The Society of Naval Architects of Japan. Japan.
3. Twenty-Second Symposiums on Naval Hydrodynamics .1999. *Propulsor Hydrodynamics/Hydro acoustics*. Commission on Physical Sciences, Mathematics, and Applications (CPSMA). Page: 110-238.
4. J. Gordon Leishman. 2002. *Principles Of HelicopterAerodynamics*. Cambridge University Press. Page: 28-40
5. Jun Ando and KuniharuNakatake. 2001. *Calculation of Three-Dimensional Unsteady Sheet Cavitation by a Simple Surface Panel Method "SQCM"*. Kyushu University, Fukuoka 812-8581, Japan.
6. Jun Ando, S. Maita and K. Nakatake. 2000. *A New Surface Panel Method to Predict Steady and Unsteady Characteristics of Marine Propeller*. Twenty-Second Symposiums on Naval Hydrodynamics.
7. Koichi Koyama,*on application of the Lifting Surface Theory of Marine Propeller*. Ship Research Institute Tokyo. Japan
8. Takashi Kanemaru and Jun Ando. 2009. *Numerical Analysis of Steady and Unsteady Sheet Cavitation on a Marine Propeller Using a Simple Surface Panel Method "SQCM"*. First International Symposium on Marine Propulsors smp'09. Norway.
9. Koichi Koyama. 2012. *Relation between the lifting surface theory and the lifting line theory in the design of an optimum screw propeller*. National Maritime Institute, Japan.
10. T. Kanemaru and Jun Ando. 2012. *Numerical Analysis Of Cavitating Propeller And Pressure Fluctuation On Ship Stern Using A Simple Surface Panel Method ''SQCM''*. Faculty of Engineering, Kyushu University, Fukuoka, Japan.
11. DavideGrassi and Stefano Brizzolara. . *Numerical Analysis of Propeller Performance by Lifting Surface Theory*. Universityof Genoa, Department of Naval Architecture and Marine Engineering, Genova, Italy.
12. Anders Smærup Olsen. 2001. *Optimization of Propeller Using the Vortex-Lattice Method*. PhD Thesis, Technical University of Denmark. Page: 17-50.
13. Anders Smærup Olsen. 2003. *Energy Coefficients for a Propeller Series*. Department of Mechanical Engineering, Technical University of Denmark, Denmark.
14. Hajime Yuasa and Norio Ishii. . *Practical Application of Discrete Vortex Element Method for Calculation of Propeller Induced Excitation Forces.* Mitsui Engineering & Shipbuilding Co., Ltd. Japan.
15. Brocklehurst and G.N.Barakos. 2012. *A Review of Helicopter Rotor Blade Tip Shapes*. CFD Laboratory, Department of Engineering, University of Liverpool, Liverpool L633GH, United Kingdom.
16. JosebaMurua. 2012. *Applications of the Unsteady Vortex-Lattice Method in Aircraft Aeroelasticity and Flight Dynamics*. Department of Aeronautics, Imperial College, London SW72AZ, United Kingdom.
17. A.R.S. Bramwell, George Done, David Balford. 2001. *Helicopter Dynamics Second Edition*. Butterworth-Heinemann, Oxford.
18. Guo-Hua Xu, Shi-Cun Wang. 2001. *Effects ofthe Shroud on Aerodynamic Performance in Helicopter Shrouded Tail*

Rotor System. Aircraft Engineering and Aerospace Technology, Vol. 73 Iss: 6, pp.568 – 573.

19. C. Young. 1976. *The Prediction of Helicopter Rotor Hover Performance using a Prescribed Wake Analysis.* Aerodynamics Dept., R.A.E., Farnborough, London.

Journal of Ocean, Mechanical and Aerospace
-Science and Engineering-, Vol.7

May 20, 2014

Palm Stearin as Alternative Binder for MIM: A Review

Amir Arifin,[a,*] Abu Bakar Sulong,[b] Gunawan,[a] Amrifan Saladin Mohruni,[a] and Irsyadi Yani,[a]

[a]*Department of Mechanical Engineering, Faculty of Engineering, Sriwijaya University, Inderalaya 30662, Indonesia*
[b]*Department of Mechanical and Material Engineering, Universiti Kebangsaan Malaysia, Selangor 43600,Malaysia*

*Corresponding author: amir_arifin@ymail.com

Paper History

Received: 5-April-2014
Received in revised form: 30-April-2014
Accepted: 8-May-2014

ABSTRACT

Palm stearin is one of the fractionation process results from palm oil that is the largest commodities in the world. It has potentially as an alternative of binder in metal injection molding based on researches that conducted in Malaysia. Palm stearin can be combined with other binder to be a binder system with the function as lubricant and surfactant in a binder system. Based on experiments showed Palm stearin has fulfilled requirement as binder in MIM such as pseudoplastic behavior from rheological test and homogeneity of the feedstock. Palm stearin can replace conventional binders that commonly used in industry.

KEY WORDS: *Palm Stearin; Natural Binder; MIM; Palm Oil.*

NOMENCLATURE

MIM	*Metal Injection Molding*
PS	*Palm Stearin*
PE	*Polyethylene*

1.0 INTRODUCTION

Production of palm oil has been increasing significantly in the recent decades. Palm Oil has successfully become one of the largest traded commodities in the world. This trend has encouraged some countries to establish research institute or organization for palm oil such as Malaysia as palm oil producing countries.

Metal Injection Molding can be categorized by net-shape process which combines injection molding and powder metallurgy [1]. MIM has advantage for produce small part with complex shape in high volume [2, 3]. MIM is comprised of several stages that should follow. Firstly is started on mixing stage, injection molding stage, debinding stage and sintering stage as shown on Fig.1. In mixing stage, metal or ceramic powder will be mixed with binder before injection process.

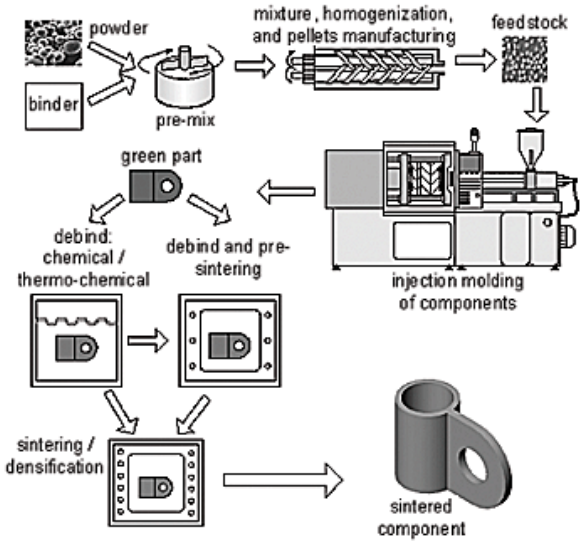

Figure 1: Metal Injection Molding process [4].

Binder has function as a vehicle for homogeneously packing of powder and keeps shape of green body after injection [5]. The selection of exact binder system for certain powder becomes critical thing to determine final product in MIM process. Other consideration that plays important in manufacturing industry is

saving cost. Using Palm Stearin as a natural binder is one of the way to reduce production costs due to Palm Stearin available in considerable amounts especially in Indonesia and Malaysia as the largest producer in the world. In this paper, the following are described with regard to Palm Stearin as alternative binder in Metal Injection Molding especially in Malaysia.

Oil palm thrives in tropical conditions with position about 5 degrees north and south along the equator line [6]. Oil palm is widely grown in several countries but the largest producers of oil Palm Indonesia and Malaysia as shown on Table 1.

Table 1: Palm Oil: World Supply and Distribution (thousand metric tons) [7]

	2008/09	2009/10	2010/11	2011/12	Mar 2012/13	Apr 2012/13
Production						
Indonesia	20,500	22,000	23,600	26,200	28,000	28,500
Malaysia	17,259	17,763	18,211	18,202	19,000	19,000
Thailand	1,540	1,345	1,288	1,546	1,700	1,700
Colombia	795	770	750	915	960	960
Nigeria	850	850	850	850	850	850
Other	3,074	3,145	3,224	3,286	3,317	3,312
Total	44,018	45,873	47,923	50,999	53,827	54,322

2.0 PALM STEARIN

Palm stearin is fraction of palm oil thorough fractionation process of palm oil. Fractionation is process to separated component in palm oil based on differences of melting point [8-10] as shown on the Fig 2. Fractionation process result of crude oil, generally consist of palm olein in liquid fraction and palm stearin in solid fraction which consist of three main groups of triglycerides. trisaturated triglycerides (*palmitate–palmitate–palmitate*); triglycerides (*palmitate–oleate–palmitate*); and polyunsaturated triglycerides (*palmitate–oleate–oleate*)[11] .

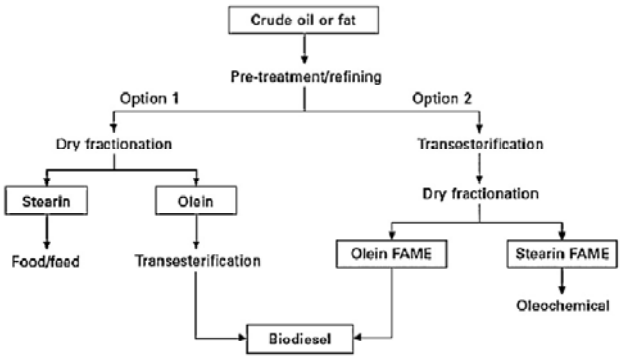

Figure 2: Fractionation of palm oil [12]

3.0 BINDER SYSTEM IN METAL INJECTION MOLDING

Binder system play critical position to determined subsequently stage in MIM, failure in one stage in MIM cannot be corrected by next stage, each stage should achieve optimal results and as small as possible to minimize the defects that occurs. Binder systems constituents for injection molding application can be divide two categorize [13]:

- Low molecular weight polymer; which has low temperature decomposition.
- High molecular weight polymer ; which has relatively high temperature decomposition

Binder system also gives strong effect to determine parameters properties of a feedstock [14]. Generally, removing binder process consists of two stages, comprising of solvent debinding and thermal debinding. A good binder system should have easy to remove in initial removal stage which usually performed using solvent [15], for example distilled water and heptanes. Remaining binder can be removed using next secondary debinding processes, which involve thermal debinding. In this stage, binder as backbone of specimen is removed. After going through a stage of debinding, specimen has behavior very fragile and circumspection is required for handling.

Ideal binder for MIM has decomposition temperature above molding and mixing temperature but has decomposition temperature before sintering temperature [5]. Palm stearin has ideal decomposition temperature as binder, starting around 200^{o}C until around 500^{o}C as shown on the Fig. 3.

Binder system in MIM process is designed based on functions as backbone, filler phase, surfactant and lubricant. Fatty acid in palm stearin is playing important role as surface active agent which required for binder system [17]. Palm stearin in binder system can be used as surfactant and lubricant. Good lubrication is required when release specimen from mold and a surfactant is necessary to connect binder and powder. A simple binder system

comprised of polyethylene and palm stearin has showed satisfactory result [17-22]. Ibrahim, *et al*. 2007, has been compared two binder system which Stearic acid was substituted by palm stearin. Palm stearin has shown good in performance that close to stearic acid value as shown on the Fig 4.

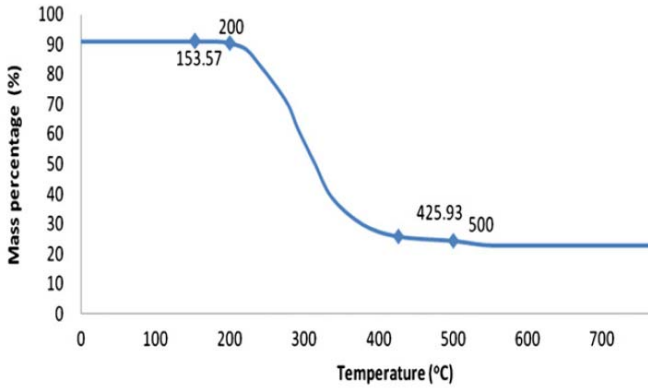

Figure 3: Thermogravimetric curve of Palm stearin [16]

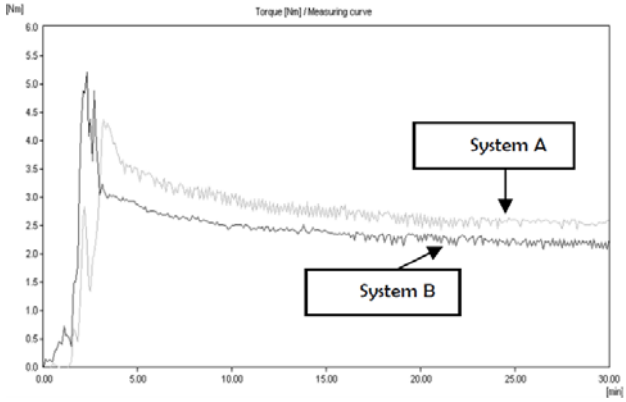

Figure 4: Comparison 2 type of Binder System: System A; polyethylene, paraffin wax and has palm stearin, System B; Polyethylene, paraffin wax, stearic acid [23].

In Biomedical material such as 316L stainless steel, Titanium alloy, palm stearin has been used as binder [20, 23-25]. Abdullah *et al* has reported that palm stearin has successful to use as binder for 316L stainless steel, feedstock 316L stainless steel exhibited homogeneity as shown on the Fig 3. System A and B has consist of Palm Stearin 10 vol%, stearic acid 10vol%, respectively. Both of system has similar composition that consists of Polyethylene 35 vol%, Paraffin wax 55vol%. Ibrahim *et al*, has used binder system with composition binder Polyethylene 40% and Palm Stearin 60% (weight percentage) for mixing with Inconel718 powder for aerospace application. Other researchers also choose 60% Palm Stearin (PS) and 40% of polyethylene (PE) as binder system composition [17, 19, 24].

Palm Stearin has shown pseudo plastic flow behavior with shear sensitivity value less than 0.5 which indicating sensitive with shear rate[22]. Rheological behavior of ZK60 Magnesium Alloy with binder 60wt.% Palm Stearin (PS) + 40wt.% polyethylene was conduct by M.R. Harun *et al*. also tend to showed pseudo-plastic fluids feedstock [21].

Percentage of palm stearin in binder system has played important role to determine viscosity and sensitivity of feedstock [24,26]. Moreover, Palm Stearin binder system has ability to coated all surface of particle and make hold tightly of particle powder as shown on Fig 5.

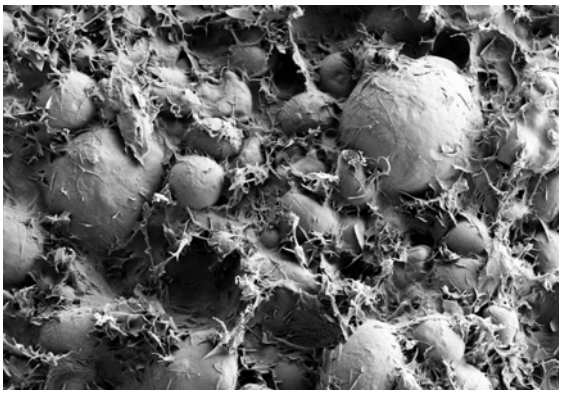

Figure 5: Stainless steel feedstock with binder system palm stearin and polyethylene, most of particle was coated by binder [24].

4.0 RHEOLOGICAL PROPERTIES

Viscosity is important issue in assess quality of feedstock, mold filling of feedstock depend on viscosity value [27]. Pseudoplastic is suitable properties of feedstock for MIM application [28, 29]. Pseudoplastic is which viscosity decreases with increase of shear rate as be defined as:

$$\eta = K\gamma^{n-1} \quad (1)$$

Where η is viscosity, K is a constant, γ, n are defined as shear rate and index of flow behavior, respectively. Flow behavior index (n) of pseudoplastic feedstock should be less than 1, since more than 1 powder and binder tend to separate when under high pressure [26, 28].

Liu *et al.*2003 reported that ideal value of shear rate in range 100 to 10000 s^{-1} with viscosity value under 1000 Pa s [30]. Rheological properties of Palm Stearin have been performed which showed satisfactory result [16,20-23,31]. A result of rheological test is used as indicators for the success of the injection process. Rheology result is showed on Fig. 6.

5.0 DEBINDING

Debinding stage is process to remove binder from injected specimen. Rapid debinding without occur defects on part is classic issues that faced by researches [32-34]. A failure to remove binder before sintering stage tend to give effect on the final result, such as, cracking, distortion and contamination [5]. Debinding for removing Palm Stearin consist of solvent and thermal processes.

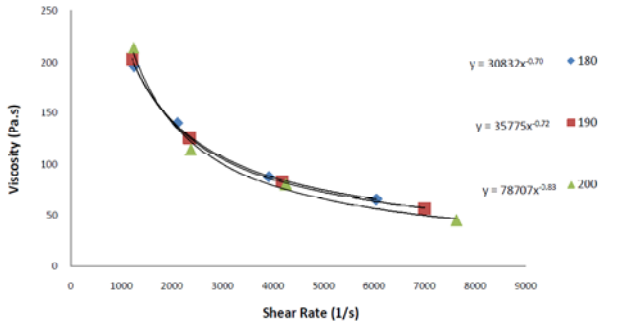

Figure 6: Viscosity vs Shear rate of feedstock using palm stearin and polyethylene as binder system at temperature 180°C, 190°C and 200°C [20].

5.1 Solvent debinding

At solvent process, injected part immersed in fluid to dissolve the Palm Stearin for subsequent binder burnout. Moreover, residual stress on specimen tend to decrease when lower molecular binder are removed [35] .Capillary path and hole are provided by palm stearin after solvent process is used to facilitate higher molecular binder out[16] as shown on Fig 7. Fick's second law generally is used to describe about mass transfer process in solvent debinding.

$$\frac{\partial c}{\partial t} = D\frac{\partial^2 C}{\partial x^2} \quad (2)$$

where C describes as concentration of diffusing substance and x is a distance of normal direction on the section.

Several researchers have been performed using heptanes to dissolves Palm Stearin from injected part [16, 23]. Ibrahim, R *et al.* 2007, has successfully to remove Palm Stearin binder system using heptane for 4 hour at 60°C and followed thermal debinding at temperature 440°C for 2 hour. Cross section thickness is playing important role to increase debinding rate [36]. Moreover, higher temperature on solvent debinding tends to increase the rate of solubility of Palm Stearin [16]. However, pore size tends not to give significant effect on debinding rate [36]. Li. Y et al 2003 has proposed about critical thickness, it have strong correlation on debinding parameters such as, particle size, holding time and powder loading, moreover critical thickness can be used as reference to design optimal debinding time without defect on the part [33].

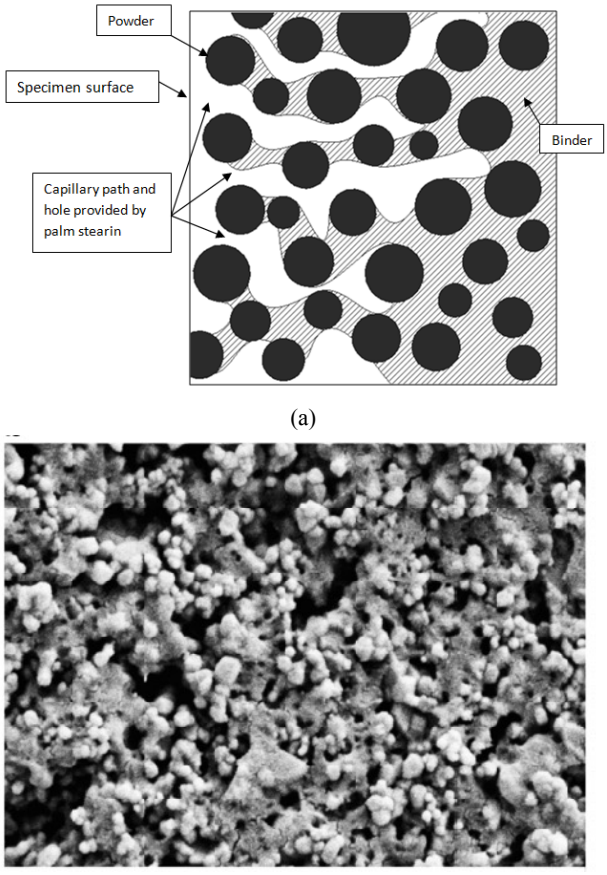

Figure 7: (a) Model of capillary path is provided after removing of palm stearin by solvent debinding, (b) Solvent debound specimen [16]

5.2 Thermal Rebinding

Thermal debinding or thermolysis has used widely in powder metallurgy industry, simplicity and ease process as consideration [33, 37]. Normally, thermal debinding is used to remove high molecular weight polymer. In thermal debinding, some events happened such as evaporation, thermal degradation, and oxidative degradation. Usually process is started on degradation of binder component into several molecular structures with various states such as gaseous, liquefied and other component evaporated directly without through degradation process [35, 38]. Degradation of binder component can be expressed as [39-41]:

$$-\frac{dh}{dt} = Kh \quad (3)$$

whereh is weight fraction of binder component/polymer, K is thermal degradation constant, which can be expressed by Arrhenius equation.

6.0 CONCLUSION

The use of palm stearin as alternative binder in Metal Injection Molding has positively impact for industry because of the availability is abundant and cheap. Moreover, as organic material Palm stearin tend to environmentally friendly which is an important added value for palm stearin. Based on several experiments, Palm stearin is candidate potentially to be alternative binder in metal injection molding industry. Several experiments have showed palm stearin has fulfilled any standard requirement that is necessary in a metal injection molding process.

ACKNOWLEDGEMENTS

The authors wish to thank the anonymous referee for constructive suggestions regarding improvement of this article.

REFERENCE

1. Huang, M.-S. and H.-C. Hsu, 2009., *Effect of backbone polymer on properties of 316L stainless steel MIM compact.* Journal of Materials Processing Technology, 209(15-16): p. 5527-5535.
2. Liu, Z.Y., et al., 2003, *Characterization of powder injection molding feedstock.* Materials Characterization, 49(4): p. 313-320.
3. Berginc, B., Z. Kampus, and B. Sustarsic, 2007, *Influence of feedstock characteristics and process parameters on properties of MIM parts made of 316L.* Powder Metallurgy, 50(2): p. 172-183.
4. Beal, V.E., C.H. Ahrens, and P.A. Wendhausen, 2004, *The use of stereolithography rapid tools in the manufacturing of metal powder injection molding parts.* Journal of the Brazilian Society of Mechanical Sciences and Engineering,. 26: p. 40-46.
5. German, R.M. and A. Bose, 1997,*Injection Molding of Metals and Ceramics*Metal Powder Industries Federation.
6. Shahidi, F., 2005, *Bailey's Industrial Oil and Fat Products, 6 Volume Set,* Wiley.
7. www.fas.usda.gov. *Palm Oil : World Supply and Distribution* 2013 [cited 2013 May 06, 2013]; Available from: www.fas.usda.gov/psdonline.
8. *http://www.palmoilworld.org*. Available from: http://www.palmoilworld.org/about_palmoil.html.
9. Zaliha, O., et al., 2004, *Crystallization properties of palm oil by dry fractionation.* Food Chemistry, 86(2): p. 245-250.
10. Norizzah, A.R., et al., 2004, *Effects of chemical interesterification on physicochemical properties of palm stearin and palm kernel olein blends.* Food Chemistry, 86(2): p. 229-235.
11. Salvi, B.L. and N.L. Panwar, 2012, *Biodiesel resources and production technologies – A review.* Renewable and Sustainable Energy Reviews, 16(6): p. 3680-3689.
12. Bart, J.C.J., N. Palmeri, and S. Cavallaro, 2010, *Biodiesel Science and Technology: From Soil to Oil*, Woodhead Publishing.
13. Aggarwal, G., et al., 2007, *Development of niobium powder injection molding. Part II: Debinding and sintering,* International Journal of Refractory Metals & Hard Materials,. 25(3): p. 226-236.
14. Ahn, S., et al., 2009, *Effect of powders and binders on material properties and molding parameters in iron and stainless steel powder injection molding process.* Powder Technology, 193(2): p. 162-169.
15. Hens, K.F. and D. Kupp, 1995, *Advanced production methods for PIM Feedstock.* Advances in Powder Metallurgy & Particulate Materials, 6: p. 45-54.
16. Mohd Foudzi, F., et al., 2013,*Yttria stabilized zirconia formed by micro ceramic injection molding: Rheological properties and debinding effects on the sintered part.* Ceramics International, 39(3): p. 2665-2674.
17. Mohamad Nor, N.H., et al., 2011, *Characterisation of Titanium Alloy Feedstock for Metal Injection Moulding Using Palm Stearin Binder System.* Advanced Materials Research, 264-265: p. 586-591.
18. Muhamad, N., et al., 2011, *Multiple Performance Optimization for the Best Injection Molding Process of Ti-6Al-4V Green Compact.* Frontiers of Manufacturing and Design Science, Pts 1-4, 44-47: p. 2707-2711.
19. Amin, S.Y.M., et al., *2011, Characterization of Feedstock Properties of PIM WC-Co with Palm Stearin Binder System*, in *5th Powder Metallurgy Symposium and Exhibition*.
20. Ramli, M.I., et al., 2012, *Powder Injection Molding of SS316L/HA Composite: Rheological Properties and Mechanical Properties of the Green Part.* Journal of Applied Sciences Research, 8(11): p. 5317-5321.
21. Harun, M.R., et al., 2010, *Rheological Investigation of ZK60 Magnesium Alloy Feedstock for Metal Injection Moulding Using Palm Stearin Based Binder System.* Applied Mechanics and Materials, 44-47: p. 4126-4130.
22. Ibrahim, R., et al., 2012, *Injection Molding of Inconel718 Parts for Aerospace Application Using Novel Binder System Based on Palm Oil Derivatives* in *World Academy of Science, Engineering and Technology*.
23. Ibrahim, R., et al., 2007, *Fabrication of 316L stainless steel parts by Injection Moulding for Biomedical Application using a Novel Binder*, in *3rd Kuala Lumpur International Conference on Biomedical Engineering 2006*, F. Ibrahim, et al., Editors. Springer Berlin Heidelberg. p. 102-105.
24. Abdullah, M.F., et al., 2011, *Comparison on Rheology Properties of Polypropylene and Polyethylene as Binder System with Stainless Steel 316L for Metal Injection Moding.* Composite Science and Technology, Pts 1 and 2, 471-472: p. 409-414.
25. Nor, N.H.M., et al.,2011, *Optimization of Injection Molding Parameter of Ti-6Al-4V Powder Mix with Palm Stearin and Polyethylene for the Highest Green Strength by Using Taguchi Method.* International Journal of Mechanical and Materials Engineering , 6, No 1: p. 126-132.
26. Karatas, C., et al., 2004, *Rheological properties of feedstocks prepared with steatite powder and polyethylene-based thermoplastic binders.* Journal of Materials Processing Technology, 152(1): p. 77-83.
27. Hausnerova, B., 2010, *Rheological characterization of powder injection molding compounds.* Polimery, 55(1): p. 3-11.

28. Huang, B., S. Liang, and X. Qu, *The rheology of metal injection molding.* Journal of Materials Processing Technology, 2003. 137(1-3): p. 132-137.
29. Wright, M., L. Hughes, and S. Gressel, 1994,*Rheological Characterization of Feedstocks for Metal Injection Molding.* Journal of Materials Engineering and Performance, 3(2): p. 300-306.
30. Liu, Z.Y., et al., 2002, *Characterization of powder injection molding feedstock.* Materials Characterization, 49(4): p. 313-320.
31. Omar, M.A., et al., 2012, *Processing of Water-atomised 316L Stainless Steel Powder UsingMetal-injection Processes.* Journal of Engineering Science, 8: p. 1-13.
32. Omar, M.A., et al., 2003, *Rapid debinding of 316L stainless steel injection moulded component.* Journal of Materials Processing Technology, 140: p. 397-400.
33. Li, Y., et al., 2003,*Critical thickness in binder removal process for injection molded compacts.* Materials Science and Engineering: A, 362(1–2): p. 292-299.
34. Tseng, W.J. and C.-K. Hsu, 1999, *Cracking defect and porosity evolution during thermal debinding in ceramic injection moldings.* Ceramics International, 25(5): p. 461-466.
35. Thian, E.S., et al., 2001, *Effects of debinding parameters on powder injection molded Ti-6Al-4V/HA composite parts.* Advanced Powder Technology, 12(3): p. 361-370.
36. Hwang, K.S., G.J. Shu, and H.J. Lee, 2005, *Solvent debinding behavior of powder injection molded components prepared from powders with different particle sizes.* Metallurgical and Materials Transactions A, 36(1): p. 161-167.
37. Liu, X.Q., et al., 2008,*Deformation behavior and strength evolution of MIM compacts during thermal debinding.* Transactions of Nonferrous Metals Society of China, 18(2): p. 278-284.
38. Liu, D.-M. and W.J. Tseng, 1999, *Binder removal from injection moulded zirconia ceramics.* Ceramics International, 25(6): p. 529-534.
39. Slade, P.E. and L.T. Jenkins, 1970, *Techniques and methods of polymer evaluation,* M. Dekker.
40. Shi, Z. and Z.X. Guo, 2004, *Kinetic modelling of binder removal in powder-based compacts.* Materials Science and Engineering a-Structural Materials Properties Microstructure and Processing, 365(1-2): p. 129-135.
41. Goswami, A., et al., 2012, *Thermal degradation kinetics of poly(trimethylol propane triacrylate)/poly(hexane diol diacrylate) interpenetrating polymer network.* Thermochimica Acta, 547: p. 53-61.

Journal of Ocean, Mechanical and Aerospace
-Science and Engineering-, Vol.7

May 20, 2014

Absorption Acid Gas Removal in Liquefied Natural Gas Process

Jaswar Koto,[a,b,*]

[a)] *Ocean and Aerospace Research Institute, Indonesia*
[b)]*Faculty of Mechanical Engineering, Universiti Teknologi Malaysia*

*Corresponding author: jaswar.koto@gmail.com

Paper History

Received: 15-April-2014
Received in revised form: 5-May-2014
Accepted: 18-May-2014

ABSTRACT

Simulation of fluid mechanic of amine absorber process in removing acid gas from feed sour gas in LNG production plant is presented in this paper. The amine absorption in the Removing Acid Gas Process is designed to remove carbon dioxide (CO_2), hydrogen sulfide (H_2S) and other sulfur compounds from the sour feed gas. The sour gas together with the recycle gas from the Treater unit enters the bottom of Amine Absorber and flows upward and passes through a demister pad to water wash section. In the Amine Absorber, the down-flowing amine solution absorbs H_2S and CO_2 from the up-flowing sour gas to produce a sweetened gas stream as a product and an amine solution rich in the absorbed acid

KEY WORDS: *Liquid Natural Gas; Acid Gas Removal; Amine Absorber; Feed Gas; Carbon Filter; Treater, Sweet Gas; Rich Amine; Water Wash System.*

NOMENCLATURE

H_2S	: Hydrogen Sulfide
CO_2	: Carbon Dioxide
MDEA	: MethylDiethanolamine
DU	: Dehydration Unit
FGS	: Flash Gas System
SRU	: Sulfur Recovery Unit
AU	: Absorption Unit
RU	: Regeneration Unit
SU	: Supporting Unit
FEED	: Front End Engineering Design
USIF	: Up-Stream Inlet Facility
FGFS	: Feed Gas Filter Separator
FPH	: Feed Pre-Heater
PFD	: Pre-Flash Drum
AA	: Amine Absorber
TU	: Treater Unit
RFD	: Rich Flash Drum
AHD	: Absorber Hydrocarbon Drum
SRD	: Solvent Recovery Drum
WWP	: Water Wash Pump WWP
WWT	: Water Wash Tray
CT	: Chimney Tray
CC	: Condensate Cooler
OW	: Overflow Weir
MWP	: Makeup Water Pump
WBT	: Water Break Tank
FWC	: Flash Wash Column
FGWWP	: Flash Gas Water Wash Pump
FGD	: Fuel Gas Drum
PF	: Pre-Filter
CF	: Carbon Filter
AF	: After-Filter
LRHE	: Lean Rich Heat Exchanger
LSBP	: Lean Solvent Booster Pump
DSHS	: De-Super Heater Steam
RB	: Re-boiler
RP	: Reflux Pump
AGAC	: Acid Gas Air Cooler
AGTC	: Acid Gas Trim Cooler
RD	: Reflux Drum
LSAC	: Lean Solvent Air Cooler
LSTC	: Lean Solvent Trim Cooler
LSP	: Lean Solvent Pump
SOP	: Skim Oil Pump
SF	: Sump Filter
SP	: Sump Pump
DPC	: Dryer Pre-Cooler

RTU : Regeneration Treating Unit
RG : Re-Generator

1.0 INTRODUCTION

Increasing global energy demand and environment issue have pushed oil and gas players to search the econ-green alternative sources even to the remote area. Energy from natural gas is the major alternative source with less environmental impact which is discovered this century. Chemical properties of the natural gas contains some complex contaminants such as CO_2, H_2S, CO, Mercaptan (Acid Gas). At the atmosphere, these materials constitute great environmental hazards for human body. They are also hindered natural gas processes.

The natural gas is effectively transported through pipelines due the energy content per unit volume is relatively low. As transportation distance increases, the pipelines system becomes inefficient; therefore liquefaction process transform from gas to liquid form is more economical and viable options.

The liquefaction of natural gas process involves operation at a very low Temperature which is about -161 ^{0}C and very low atmospheric pressure. At these conditions CO_2 can freeze out on exchanger surface, plugging lines and reduce plant efficiency. Therefore there is need for removal of CO_2 before liquefaction process, this is done not to overcome the process bottle necks but also to meet the LNG product specifications, prevent corrosion of process equipment and environmental performance.

Amine gas treating is also known as gas sweetening and acid gas removal. The acid gas removal unit in LNG process is designed to remove unnecessary gases such as:$H_2S$and CO_2 and other sulphur compounds from the FEED sour gas by means of chemical absorption. There are many acid gas treating processes available for removal of CO2 from natural gas. These processes include Chemical solvents, Physical solvents, Adsorption Processes Hybrid solvents and Physical separation (Membrane) (Kohl and Nielsen, 1997); The chemical solvents and physical solvents or combination of these two have been used extensively in existing base load LNG facilities (David Coyle et. al 2003).

The process scheme selected in the present study is MDEA. In the process scheme, the treated gas is sent to DU, the flash gas is sent to FGS, and the acid gas is sent to SRU.

The MDEA is a tertiary amine and an “activator”. The amine reactions occurring in the absorber are:

$$H_2S + R_2CH_3N \rightarrow R_2CH_3NH^+ + HS^- \quad (1)$$

$$CO_2 + R_2CH_3N + H_2O \rightarrow R_2CH_3NH^+ + HCO_3^- \quad (2)$$

The H_2S reacts much faster with the amine than does the CO_2, because the reaction between amine and H_2S appears gas film diffusion-rate limited, whereas the reaction between the amine and CO_2 is kinetically limited. Therefore, if the absorber is designed in such a manner to provide an adequate number of contact stages with sufficient contact time, total absorption of H_2S and CO_2 can be achieved. The trays in the absorber are designed with sufficient contact time such that the CO_2 content of the sweet gas meets the 25 ppmv specification while also achieving the 2 ppmv H_2S specification. The activator present in the solvent enhances the CO_2 reaction kinetics, enabling its essentially complete removal.

To achieve low H_2S and CO_2 slippage in the absorber operating at high pressure, it is necessary to strip the amine to a very low acid gas loading (typical loading is < 0.01 mole acid gas/mole amine). Steam stripping occurs in the regenerator at high temperature and reverses the reactions given above. The steam reduces the partial pressure of H_2S and CO_2 over the amine, thus reducing the equilibrium concentration (or loading) of these components in the amine.

2.0 ABSORPTION ACID GAS PROCESS FLOW

The acid gas removal or amine gas treating process is divided into three main units as follows: AU, RU and SU. In the absorber, the down-flowing amine solution absorbs H_2S and CO_2 from the up-flowing sour gas to produce a sweetened gas stream as a product and an amine solution rich in the absorbed acid gases. Fig.1 shows an absorption unit process flow diagram for acid gas removal. The resultant “rich” amine is then routed into the regenerator to produce regenerated or “lean” amine that is recycled for reuse in the absorber. The stripped overhead gas from the regenerator is concentrated H_2S and CO_2.

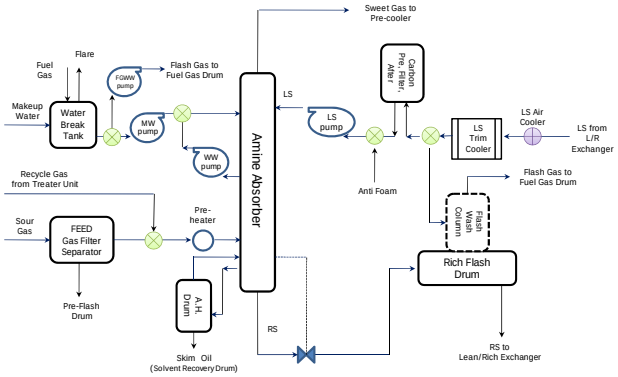

Figure 1: Absorption removing acid gas process flow diagram

2.1 Feed Gas Filtration and Preheating Process

The feed gas filtration and preheating mainly consists of FGFS and FPH. The sour feed gas with composition as shown Table.1 is flown from the USIF to the FGFS. The main task of FGFS eliminates any liquid hydrocarbons droplets and solids. Another task of the FGFS is to handle liquid slugs and shuts down the train when a high liquid level occurs. The liquid from the drum is recycled back to the PFD in the USIF.

In order to avoid liquid hydrocarbon condensing in the AA, the outlet gas from the FGFS is combined with the recycle gas, as shown in Table.1, from TU before entering the FPH to maintain the gas above its saturation temperature (dew point). Normal operating temperature and Pressure is 40.0^0C and 69 bar prior to entering Absorber as shown in Table.2 in In-AA. The FPH uses MP steam as a heating medium.

Table 1: Properties of the feed gas and recycle gasses.

Items	Feed Gas to FGFS	Recycle Gas from TU
State	Vapor	Vapor
$H_2S\ (mol\ \%\ dry)$	0.8	0.0
$CO_2\ (mol\ \%\ dry)$	2.5	0.0
$Sulfur\ (mol\ \%\ dry)$	0.04	0.02
$Molecular\ (Wet)$	19.0	18.0
$Density\ (kg/m^3)$	57.0	48.0
Normal Operating Temperature (C)	40^0	60^0
Normal Operating Pressure (Bar)	73	70
$Total\ flow\ kg/h\ (wet)$	1460000	32000

Table 2: Mechanical properties of feed gas enters and Rich Solvent leaves the Amine Absorber

Items	Feed Gas from FGFS to AA
State	Vapor
$H_2S\ (mol\ \%\ dry)$	0.8
$CO_2\ (mol\ \%\ dry)$	2.40
$Sulfur\ (mol\ \%\ dry)$	0.04
$Molecular\ (Wet)$	19.0
$Density\ (kg/m^3)$	57.0
Normal Operating Temperature (C)	40^0
Normal Operating Pressure (Bar)	69
$Total\ flow\ kg/h\ (wet)$	1490000

2.2 Amine Absorption System

The absorption process mainly consists of the following equipments: Amine Absorber, Flash Wash Column, Lean Solvent Pump, Water Wash Pump, Makeup Water Pump, Flash Gas Water Wash Pump, Absorber Hydrocarbon Drum, Rich Flash Drum and Water Break Tank.

The feed gas with mechanical properties as shown in Table.2 enters the bottom of AA and flows upward and passes through a demister pad to water wash section. Amine Absorber is equipped with 30 absorption trays, where the gas is counter-currently contacted with the solvent. The lean solvent enters the tower at a controlled temperature of 45^0C through a liquid distributor and flows down through the trays, absorbing H_2S and CO_2 to the required product specifications. Only a small amount of mercaptans and other sulfur compounds are absorbed by the solvent.

As the solvent flows down through absorber, the heat of absorption liberated by the acid gases reacting with the solvent is removed by the solvent. Thus, the rich solvent leaves the bottom of the column at an elevated temperature around 66^0C as shown in Table.2.

A solvent reservoir is maintained in the bottom of AA by liquid level control with an automatic level control valves in the rich solvent line between AA and RFD. Pressure differential indicators are also available so that the pressure drop and hydraulic performance of AA can be monitored.

AHD is provided adjacent to the bottom of AA to allow liquid hydrocarbon skimming capabilities in AA, when necessary, to the SRD.

The top section of AA contains three WWT and an OW above the lean solvent feed point to minimize solvent losses. A pump-around loop is used for the wash water to provide good gas or liquid contacting. A portion of the makeup water enters at the pump-around pump discharge.

The makeup water at 45^0C and 3.5 bar from the CC and fuel gas are stored in the WBT. The water streams enter above the top WWT, and then, the make-up water is flown to MWP and FGWWP. Mechanical properties of the makeup water are shown in Table.3.

Table 3: Mechanical properties of make-up water from WBT to MWP and FGWWP

Items	Make-up water from WBT to MWP	Make-up water from WBT to FGWWP
State	Liquid	Liquid
$H_2S\ (mol\ \%\ dry)$	0.0	0.0
$CO_2\ (mol\ \%\ dry)$	0.0	0.0
$Sulfur\ (mol\ \%\ dry)$	0.00	0.00
$Molecular\ (Wet)$	18.0	18.0
$Density\ (kg/m^3)$	997.0	997.0
Normal Operating Temperature (C)	45^0	45^0
Normal Operating Pressure (Bar)	1.2	1.2
$Total\ flow\ kg/h\ (wet)$	3800	1130

WWP draws water from the CT and pumps the water to combine with a portion of the makeup water from MWP. The mechanical properties of the waters are shown in Table.4. The makeup water entering at this location reduces the build-up of solvent in the water wash loop. The water wash minimizes the losses of solvent with the sweet gas. Water level above the chimney tray is maintained with an automatic level control valve, which sends excess water to RFD

The sweet gas from top of AA is flown to DPC in RTU with expected parameters as shown in Table.5

Table 4: Mechanical properties of water withdrawn from the chimney tray

Items	Water from CT-AA to WWP	Combination water from WWP-MWP to WWT-AA
State	Liquid	Liquid
$H_2S\ (mol\ \%\ dry)$	1.1	1.15
$CO_2\ (mol\ \%\ dry)$	2.8	2.8
$Sulfur\ (mol\ \%\ dry)$	0.00	0.00
$Molecular\ (Wet)$	18.0	18.0
$Density\ (kg/m^3)$	990.0	991.0
Normal Operating Temperature (C)	47^0	46^0
Normal Operating Pressure (Bar)	69	69
$Total\ flow\ kg/h\ (wet)$	67800	68000

Table 5: Mechanical properties of sweet sour gas from Amine Absorber

Items	Sweet Gas from AA
State	Vapor
$H_2S\ (mol\ \%\ dry)$	0.0
$CO_2\ (mol\ \%\ dry)$	0.0
$Sulfur\ (mol\ \%\ dry)$	0.035
$Molecular\ (Wet)$	18.4
$Density\ (kg/m^3)$	52.0
Normal Operating Temperature (C)	47^0
Normal Operating Pressure (Bar)	68.0
$Total\ flow\ kg/h\ (wet)$	1385000

The rich solvent flows from the bottom of AA to RFD with mechanical properties of the rich solvent are shown in Table.6. The RFD serves two purposes:

i. Degassing of volatile, dissolved hydrocarbons; and
ii. Separation of heavier liquid hydrocarbons.

Table 6: Mechanical properties of feed gas enters and Rich Solvent leaves the Amine Absorber

Items	Rich Solvent from AA to RFD	Foam Water to FWC
State	Liquid	Liquid
$H_2S\ (mol\ \%\ dry)$	7.0	7.1
$CO_2\ (mol\ \%\ dry)$	21.9	21.8
$Sulfur\ (mol\ \%\ dry)$	0.0	0.0
$Molecular\ (Wet)$	29.0	29.0
$Density\ (kg/m^3)$	1055.0	1055.0
Normal Operating Temperature (C)	66^0	45^0
Normal Operating Pressure (Bar)	69	7.0
$Total\ flow\ kg/h\ (wet)$	1680000	8200

Hydrocarbon skimming is provided to allow liquid hydrocarbon withdrawal when necessary to the SRD. A small water flow from FGWWP enters above the top packed bed of FWC to wash the flash gas and minimize solvent losses. Also the water stream has a Chemical Injection Point to allow the introduction of antifoam when required.

The flashed gas exiting FWC is water saturated at 42^0C and 6.8 Bar and is routed to the FGD. The Flash Gas exits the RFD through a three bed packed FWC. Since the flashed gas contains too much H_2S for the fuel system, the gas is contacted with a slipstream of the lean solvent to meet the requirement of less than 50 ppmv H_2S. The cooled lean solvent enters above the middle packed bed to re-absorb most of the H_2S and a portion of the CO_2 flashed out of the solvent in the drum.

2.3 Carbon Filtration Process

Filtration section consists of the following equipments: Pre-Filter, Carbon-Filter and After-Filter as shown in Fig.2. A 25% slipstream is routed to a filtration section. The mechanical properties are shown in the Table.7. PF removes any solid materials which may be in the system and protects CF from plugging. CF will remove surface active contaminants that promote foaming such as heavy hydrocarbons, surfactants, compressor oils, etc. Downstream of CF is AF to ensure that carbon fines from CF do not contaminate the system. Such carbon fines could be the result of improper CF operation, such as inadequate carbon defining, aging of the carbon, or improper installation. PF and AF are cartridge filters, rated at 10 micron.

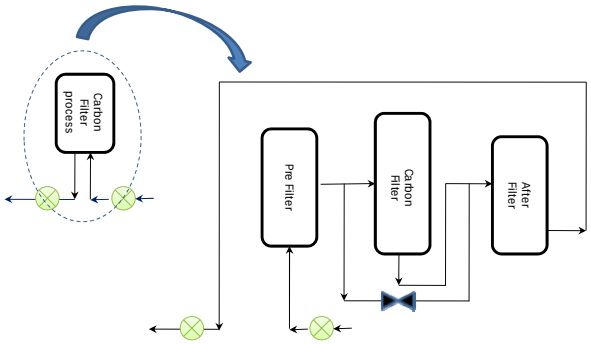

Figure 2: Carbon filter flow diagram.

Table.7 Mechanical properties of sweet sour gas to Carbon filter section.

Items	Stream to CF section
State	Liquid
$H_2S\ (mol\ \%\ dry)$	0.15
$CO_2\ (mol\ \%\ dry)$	0.60
$Sulfur\ (mol\ \%\ dry)$	0.00
$Molecular\ (Wet)$	29.0
$Density\ (kg/m^3)$	1009.0
Normal Operating Temperature (C)	45^0
Normal Operating Pressure (Bar)	8.0
$Total\ flow\ kg/h\ (wet)$	398,000

3.0 CONCLUSION

Absorption acid gas removal of Liquefied Natural Gas process has been discussed. The process includes FEED gas filtration and preheating process, amine absorption system and carbon filtration process**.**

ACKNOWLEDGEMENTS

The author would like to convey a great appreciation to Ocean and Aerospace Research Institute, Indonesia and faculty of mechanical engineering, Universiti Teknologi Malaysia for supporting this research.

REFERENCES

1. Carroll, John, J., Maddocks, James, R. (1999), "Design Considerations for Acid Gas Injection, *Laurence Reid Gas Conditioning Conference*.
2. Jaswar, (2010), "Study on Mechanical Process Facility of Floating LNG Vessel," *Asia Pacific Offshore Conference, Vol.1*, Kuala Lumpur, Malaysia.
3. Jaswar, (2010), " EPC Floating LNG Using UTM's NAOE Tool," *Asia Pacific Offshore Conference, Vol.1*, Kuala Lumpur, Malaysia.

4. Jaswar, Mazlan, Nofrizal, Junaidi, Azwadi, Agoes, Zamani, Adi, Affendy, Zaidi, Fluid Simulation of Absorption Acid Gas Removal Process in Floating LNG Production Vessel, *Asian International Conference of Fluid Mechanic*, November, 2011, Chennai, India.
5. Jaswar, Mazlan, Nofrizal, Junaidi, Azwadi, Agoes, Zamani, Adi, Affendy, Zaidi, Fluid Simulation of Regeneration Acid Gas Removal Process in Floating LNG Production Vessel, *Asian International Conference of Fluid Mechanic*, November, 2011, Chennai, India.
6. Salako Abiodun Ebenezer, J. S. Gudmundsson, (2005), "Removal of Carbon Dioxide from Natural Gas Production for LNG Production", *Project Report, Institute of Petroleum Technology Norwegian University of Science and Technology.*

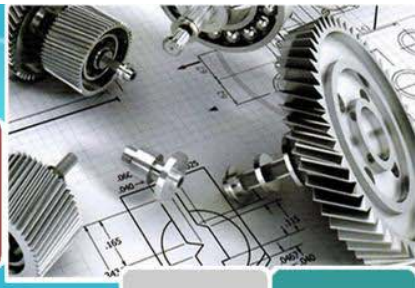

Call for Papers

Ocean, Mechanical and Aerospace Scientists and Engineers (OMAse) Conference

Deadlines

1. Abstract submission : July, 20th, 2014
2. Notice of acceptance : August 1th, 2014
3. Paper submission : October 1th, 2014
4. Conference date : November 19-20 th, 2014

Submmission

email :isomase.org@gmail.com

1. Members of ISOMAse : $ 70
2. Non member : $ 100
2. Students : $ 30

Please visit to following website :
http://isomase.org/OMAse_2014.php

Organized by :

International Society of Ocean, Mechanical and Aerospace Scientists and Engineers

UTM RESEARCH UNIVERSITY
Faculty of Mechanical Engineering
Universiti Teknologi Malaysia

Faculty of Engineering
Universitas Riau

Chairman

Jaswar Koto (Ocean and Aerospace Research Institute, Indonesia
Universiti Teknologi Malaysia, Malaysia)

Committee

Adhy Prayitno (Universitas Riau, Indonesia)
Adi Maimun (Universiti Teknologi Malaysia, Malaysia)
Agoes Priyanto (Universiti Teknologi Malaysia, Malaysia)
Ahmad Fitriadhy (Universiti Malaysia Terengganu, Malaysia)
Ahmad Zubaydi (Institut Teknologi Sepuluh Nopember, Indonesia)
Buana Ma'ruf (Badan Pengkajian dan Penerapan Teknologi, Indonesia)
Carlos Guedes Soares (Centre for Marine Technology and Engineering,-
(CENTEC) University of Lisbon, Portugal)
Cho Myung Hyun (Kiswire Ltd, Malaysia)
Dani Harmanto (University of Derby, UK)
Harifuddin (DNV, Batam, Indonesia)
Iis Sopyan (International Islamic University Malaysia, Malaysia)
Jamasri (Universitas Gadjah Mada, Indonesia)
Mazlan Abdul Wahid (Universiti Teknologi Malaysia, Malaysia)
Moh Hafidz Efendy (PT McDermott, Indonesia)
Mohamed Kotb (Alexandria University, Egypt)
Priyono Sutikno (Institut Teknologi Bandung, Indonesia)
Sergey Antonenko (Far Eastern Federal University, Russia)
Sunaryo (Universitas Indonesia, Indonesia)
Sutopo M (PT Saipem, Indonesia)
Tay Cho Jui (National University of Singapore, Singapore)
Tris Zulfirmie (PT Mubadala Petroleum, Indonesia)

Scope

The ISOMAse welcomes manuscript submissions from academicians, scholars, and practitioners for possible publication from all over the world that meets the general criteria of significance and educational excellence. The scope of the conference is as follows:

- Environtment and Safety
- Renewable Energy
- Naval Architect and Offshore Engineering
- Computational and Experimental Mechanics
- Hydrodynamic and Aerodynamics
- Noise and Vibration
- Aeronautics and Satellite
- Engineering Materials and Corrosion
- Fluids Mechanics Engineering
- Stress and Structural Modeling
- Manufacturing and Industrial Engineering
- Robotics and Control
- Heat Transfer and Thermal
- Power Plant Engineering
- Risk and Reliability
- Case studies

Venue

Hotel Resty Menara
Jl. Sisingamangaraja No. 89
Pekanbaru
Riau-Indonesia

Published & Printed

ISOMAse
Resty Menara Hotel
Jalan Sisingamangaraja No.89
Pekanbaru-Riau, Indonesia
http://www.isomase.org/

Teknik Mesin
Fakultas Teknik
Universitas Riau,
Indonesia
http://ft.unri.ac.id/

ISSN: 2354-7065